The complementary relationship in estimation of regional evapotranspiration: The Complementary Relationship Areal Evapotranspiration and Advection-Aridity models

Michael T. Hobbins and Jorge A. Ramírez
Department of Civil Engineering, Colorado State University, Fort Collins, Colorado

Thomas C. Brown
Rocky Mountain Research Station, U.S. Forest Service, Fort Collins, Colorado

Lodevicus H. J. M. Claessens
The Ecosystems Center, Marine Biological Laboratory, Woods Hole, Massachusetts

Abstract. Two implementations of the complementary relationship hypothesis for regional evapotranspiration, the Complementary Relationship Areal Evapotranspiration (CRAE) model and the Advection-Aridity (AA) model, are evaluated against independent estimates of regional evapotranspiration derived from long-term, large-scale water balances (1962–1988) for 120 minimally impacted basins in the conterminous United States. The CRAE model overestimates annual evapotranspiration by 2.5% of mean annual precipitation, and the AA model underestimates annual evapotranspiration by 10.6% of precipitation. Generally, increasing humidity leads to decreasing absolute errors for both models, and increasing aridity leads to increasing overestimation by the CRAE model and underestimation by the AA model, with the exception of high, arid basins, where the AA model overestimates evapotranspiration. Overall, the results indicate that the advective portion of the AA model must be recalibrated before it may be used successfully on a regional basis and that the CRAE model accurately predicts monthly regional evapotranspiration.

1. Introduction

In problems of regional hydrology, and therefore of global climatology, understanding the large-scale behavior of processes defining fluxes of sensible and latent heat is of paramount importance. In estimating evapotranspiration, the physics of energy and mass transfer at the land surface–atmosphere interface can be successfully modeled at small temporal and spatial scales [*Parlange and Katul*, 1992a, 1992b], yet our understanding of the processes at the monthly, or seasonal, and regional scales necessary for use by hydrologists, water managers, and climate modelers is limited.

Consequently, our ability to estimate actual regional evapotranspiration (ET_a) is often constrained by models that treat potential evapotranspiration (ET_p) as an independent climatic forcing process, often an empirical function of pan evaporation (ET_{pan}) observed at nearby weather stations, or by models that tend to rely on gross assumptions as to the nature of moisture dynamics in each of the components of the land surface–atmosphere interface and of the interactions between them. However, at regional scales, ET_a and ET_p are not independent of each other. Complex feedback interactions between processes governing their rates are established based on the degree to which the soil can satisfy the atmospheric demand for water vapor and on the resultant effect on energy distribution at the land-atmosphere interface. There is therefore a need for models of regional evapotranspiration that incorporate these feedback mechanisms, while avoiding the difficulties inherent in explicitly coupling the microscale (surface) and macroscale (free atmosphere) phenomena in the soil-plant-atmosphere system. Complementary relationship models are such models. The hypothesis of the complementary relationship between ET_a and ET_p in regional evapotranspiration was first proposed by *Bouchet* [1963]. Using such models, ET_a is estimated using data that describe the conditions of the overpassing air, obviating the need for locally optimized coefficients and surface parameterizations.

The most widely known of these models are the Complementary Relationship Areal Evapotranspiration (CRAE) model [*Morton*, 1983] and the Advection-Aridity (AA) model [*Brutsaert and Stricker*, 1979]. In earlier versions of the CRAE model [*Morton*, 1976], good agreement was shown between model estimates and water budget estimates of regional evapotranspiration (ET_a) for basins in Canada, Ireland, Kenya, and the United States. However, these versions predicted potential evapotranspiration (ET_p) with the Penman equation and did not invoke the assumption of an "equilibrium temperature" T_p. The version used in the work reported herein was calibrated by *Morton* [1983] on a monthly basis and applied on an annual basis to 143 basins in Canada, the United States, Ireland, Africa, Australia, and New Zealand. The mean absolute error of 19.6 mm yr^{-1} convinced *Morton* [1983, p. 34] that "[T]he environmental diversity, the calibration technique, and the good fit of average annual data . . . combine to provide

Copyright 2001 by the American Geophysical Union.

Paper number 2000WR900358.
0043-1397/01/2000WR900358$09.00

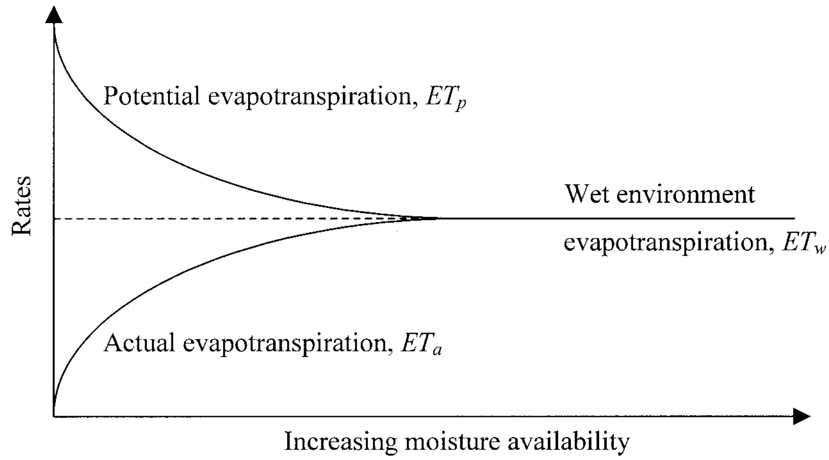

Figure 1. Schematic representation of the complementary relationship in regional evapotranspiration (assuming constant energy availability).

assurance that the monthly estimates of areal evaporation are realistic."

The Advection-Aridity model was used by *Brutsaert and Stricker* [1979] to calculate regional evapotranspiration over time steps of 3 days for a small, rural catchment in the Netherlands during the drought of 1976, when ET_p far exceeded ET_a. The model was found to yield a good match with energy budget estimates. However, the AA model has not been tested on a continental-scale basis, over a wide variety of climates, nor on a monthly basis, all features which are essential in hydrological and climatological modeling.

Aside from *Morton*'s [1965, 1983] and *Morton et al.*'s [1985] numerous publications, several studies have addressed the validity of complementary relationship models, whether through comparison with other evapotranspiration estimators [*Ben-Asher*, 1981; *Sharma*, 1988; *Doyle*, 1990; *Lemeur and Zhang*, 1990; *Chiew and McMahon*, 1991; *Parlange and Katul*, 1992a], through analysis based on meteorological observations and/or modeling results [*LeDrew*, 1979; *McNaughton and Spriggs*, 1989; *Granger and Gray*, 1990; *Lhomme*, 1997; *Kim and Entekhabi*, 1997], or by defining improvements to existing models [*Kovacs*, 1987; *Granger*, 1989; *Parlange and Katul*, 1992b]. Although these studies demonstrated varied success for complementary relationship models, the hypothesis is considered an important concept for hydrologic modeling [*Nash*, 1989; *Dooge*, 1992]. However, with the exception of *Morton* [1983] none of these studies evaluated the complementary relationship over a wide range of climatologically varying conditions (e.g., continental size areas); thus its value as an operational tool has not been well established.

This study compares the CRAE model to the AA model regarding formulation and performance, and, most important, it evaluates the complementary relationship hypothesis in the context of large-scale, long-term water balances. Specifically, the authors sought to (1) construct monthly surfaces for the conterminous United States of the components of the complementary relationship using the CRAE [*Morton*, 1983; *Morton et al.*, 1985] and AA [*Brutsaert and Stricker*, 1979] models; (2) examine the spatial distribution of these surfaces across the conterminous United States; (3) compare the models' estimates of actual evapotranspiration to independent estimates of regional evapotranspiration provided by long-term, large-scale water balances for undisturbed basins in the conterminous United States; and (4) examine the errors invoked in closing the water balances and the relationships of these closure errors to climatological and physical basin characteristics.

2. Complementary Relationship

2.1. Complementary Relationship Hypothesis

Bouchet's [1963] hypothesis of a complementary relationship states that over areas of a regional size and away from sharp environmental discontinuities, there exists a complementary feedback mechanism between actual (ET_a) and potential (ET_p) evapotranspiration. In this context, ET_p is defined as the evapotranspiration that would take place from a moist surface under the prevailing atmospheric conditions, limited only by the amount of available energy. Under conditions where ET_a equals ET_p, this rate is referred to as the wet environment evapotranspiration (ET_w). The general complementary relationship is then expressed as

$$ET_a + ET_p = 2ET_w. \quad (1)$$

The complementary relationship hypothesis is essentially based on empirical observations, supported by a conceptual description of the underlying interactions between evapotranspiring surfaces and the atmospheric boundary layer. *Bouchet* [1963] hypothesized that when, under conditions of constant energy input to a given land surface–atmosphere system, water availability becomes limited, ET_a falls below its potential, and a certain amount of energy becomes available. This energy excess, in the form of sensible heat and/or long wave back radiation, increases the temperature and humidity gradients of the overpassing air and leads to an increase in ET_p equal in magnitude to the decrease in ET_a. If water availability is increased, the reverse process occurs, and ET_a increases as ET_p decreases. Thus ET_p ceases to be an independent causal factor, or climatologically constant forcing function, and instead is predicated upon the prevailing conditions of moisture availability. Figure 1 illustrates the complementary relationship. For a more detailed analysis of this hypothesis, see *Bouchet*'s [1963] seminal paper.

2.2. Advection-Aridity Model

In examining the CRAE and AA models, it will be useful to bear in mind *Penman*'s [1948] list of the two requirements for evaporation: first, the mechanism for removing the water vapor, or sink strength, and, second, supply of energy to provide the latent heat of vaporization, or energy balance.

The AA model combines, first, bulk mass transfer and, second, energy budget considerations in a convex linear combination of terms representing these two phenomena in the familiar Penman expression for evaporation from a wet surface, or potential evapotranspiration ET_p^{AA}:

$$\lambda ET_p^{AA} = \frac{\Delta}{\Delta + \gamma} Q_n + \lambda\left(\frac{\gamma}{\Delta + \gamma}\right) E_a. \tag{2}$$

The first term of (2) represents a lower limit on the evaporation from moist surfaces, as the second term tends toward zero over large, homogeneous surfaces under steady state conditions. The second term represents the effects of large-scale advection. Here λ represents the latent heat of vaporization, Δ is the slope of the saturated vapor pressure curve at air temperature, γ is the psychrometric constant, and Q_n is the net available energy at the surface, usually approximated by the net absorbed radiation at the surface minus the diffusive ground heat flux, $R_n - G$. E_a is known as the "drying power of the air" and is a product of a function of the wind speed at height Z_r above the evaporating surface, or "wind function" $f(U_r)$, and the difference between the saturated vapor pressure (e_a^*) and vapor pressure of the overpassing air (e_a), or "vapor pressure deficit." E_a takes the following general form:

$$E_a = f(U_r)(e_a^* - e_a). \tag{3}$$

The AA model uses a simple, empirically based, linear approximation for the wind function $f(U_r)$ proposed by *Penman* [1948]:

$$f(U_r) \approx f(U_2) = 0.26(1 + 0.54U_2)\eta. \tag{4}$$

The original expression, $f(U_2) = 0.26\ (1 + 0.54\ U_2)$, required wind speeds at 2-m elevation in m s^{-1} and vapor pressures in mbars to yield E_a in mm d^{-1}. The factor η in (4) is required to produce dimensional homogeneity in the SI system. Substituting this approximation and (3) into the Penman equation (2) yields the expression for ET_p^{AA} in (5) used by *Brutsaert and Stricker* [1979] in the original AA model:

$$\lambda ET_p^{AA} = \frac{\Delta}{\Delta + \gamma} Q_n + \lambda \frac{\gamma}{\Delta + \gamma} f(U_2)(e_a^* - e_a). \tag{5}$$

In formulating the AA model for use in 3-day time steps, *Brutsaert and Stricker* [1979] ignore any effect of atmospheric instability in the wind function term.

In their original model, *Brutsaert and Stricker* [1979] calculated ET_w^{AA} over 3-day periods using the *Priestley and Taylor* [1972] equation for partial equilibrium evaporation:

$$\lambda ET_w^{AA} = \alpha \frac{\Delta}{\Delta + \gamma} Q_n, \tag{6}$$

where the value of the constant α is 1.28. The value of this constant and its influence on the performance of the AA model are examined by *Hobbins et al.* [this issue].

2.3. Complementary Relationship Areal Evapotranspiration Model

Morton [1983] states that for nonhumid environments both the Penman approach and the improvements to it suggested by *Kohler and Parmele* [1967], that the net radiation term can be better estimated using an approximation to the surface temperature by expanding the back radiation (long wave radiation) term about the air temperature T_a, lead to inaccurate estimates of the energy available for evaporation.

To calculate ET_p using the so-called "climatological approach," *Morton* [1983] decomposes the Penman equation into two separate equations describing the energy balance and vapor transfer process. The refinement proposed by *Kohler and Parmele* [1967] is developed further by the use of an "equilibrium temperature" T_p. T_p is defined as the temperature at which *Morton*'s [1983] energy budget method and mass transfer method for a moist surface yield the same result for ET_p, and it is used to adjust the surface energy budget for differences in back radiation ΔLW and sensible heat ΔH as follows:

$$ET_p|_{T=T_p} = ET_p|_{T=T_a} - \frac{\Delta LW + \Delta H}{\lambda}. \tag{7}$$

In (7), ΔLW is approximated by a first-order Taylor expansion of the black body radiation about T_p:

$$\Delta LW = 4\epsilon\sigma T_p^3(T_p - T_a), \tag{8}$$

where ϵ represents the emissivity of the evaporating surface and σ represents the Stefan-Boltzmann constant. The psychrometric constant γ can be expressed as

$$\gamma = \frac{pC_p}{0.622\lambda} = \beta \frac{e_p - e_a}{T_p - T_a} = \frac{H}{\lambda ET} \frac{e_p - e_a}{T_p - T_a}, \tag{9}$$

where β is the Bowen ratio, the ratio of sensible heat flux H to latent heat flux λET; p is pressure, and C_p is the specific heat of air at constant pressure. ΔH can be then expressed as

$$\Delta H = f_T(T_p - T_a). \tag{10}$$

In his formulation of the CRAE model, *Morton* [1983] replaced the wind function $f(U_r)$ with a calibrated vapor transfer coefficient f_T defined in (11) below, which is constant for a given atmospheric pressure and independent of wind speed:

$$\lambda f(U_r) \approx f_T = (p_0/p)^{0.5} f_Z \zeta^{-1}. \tag{11}$$

Morton [1983] assumes f_T to be independent of wind speed for the following reasons. First, vapor transfer increases with both surface roughness and wind speed, but these two are negatively correlated; vapor transfer increases with atmospheric instability, which is more pronounced at lower wind speeds. *Morton* [1983] assumes that as a result of these two complementary mechanisms, no net change in vapor transfer occurs because of variations in wind speed. Second, *Morton* [1983] questions the reliability of climatological observations of wind speed because of instrumental and station variability. In (11), ζ represents a dimensionless stability factor with values greater than or equal to 1, p is the atmospheric pressure, and p_0 is the atmospheric pressure at sea level. Here f_Z is a coefficient whose value is 28.0 W m^{-2} mbar^{-1} for above-freezing temperatures. For below-freezing temperatures the value of f_Z is increased by a factor of 1.15, the ratio of the latent heat of sublimation to the latent heat of vaporization. The exponent 0.5 represents the effect of atmospheric pressure on the evapotranspiration process and the vapor transfer coefficient. Combining the expressions for ΔLW and ΔH and substituting f_T yields *Morton*'s [1983] energy budget (12) and mass transfer (13) expressions for ET_p^{CRAE} at the equilibrium temperature T_p:

$$\lambda \mathrm{ET}_p^{\mathrm{CRAE}} = Q_n - [\gamma f_T + 4\varepsilon\sigma T_p^3](T_p - T_a), \qquad (12)$$

$$\lambda \mathrm{ET}_p^{\mathrm{CRAE}} = f_T(e_p^* - e_a). \qquad (13)$$

In (13), e_p^* is the saturated vapor pressure at T_p, and e_a is the actual vapor pressure at T_a. $\mathrm{ET}_p^{\mathrm{CRAE}}$ is then defined as the evapotranspiration that would take place at T_p.

Morton [1983] modifies the Priestley-Taylor partial equilibrium evaporation equation (6) to account for the temperature dependence of both the net radiation term and the slope of the saturated vapor pressure curve Δ. The Priestley-Taylor factor α is replaced by a smaller factor $b_2 = 1.20$, while the addition of $b_1 = 14$ W m^{-2} accounts for large-scale advection during seasons of low or negative net radiation and represents the minimum energy available for ET_w but becomes insignificant during periods of high net radiation. As in the $\mathrm{ET}_p^{\mathrm{CRAE}}$ expression (12), disparities between the surface temperature and the air temperature at potential conditions are considered by subtracting ΔLW (8) from the radiation budget at the surface. $\mathrm{ET}_w^{\mathrm{CRAE}}$ is calculated as

$$\lambda \mathrm{ET}_w^{\mathrm{CRAE}} = b_1 + b_2 \frac{\Delta p}{\Delta_p + \gamma} [Q_n - 4\varepsilon\sigma T_p^3(T_p - T_a)]$$

$$= b_1 + b_2 \frac{\Delta_p}{\Delta_p + \gamma} Q_n^*, \qquad (14)$$

where Δ_p and Q_n^* are the slope of the saturated vapor pressure curve and the net available energy adjusted to the equilibrium temperature T_p, respectively.

Although some writers have claimed that one of the advantages of the CRAE model is that it does not require any calibration of parameters, this is only true in a local sense. The CRAE model incorporates global calibration of parameters b_1, b_2, and f_T, using data collected in arid regions for 154 station months with precipitation totals sufficiently small that they could be substituted for ET_a [*Morton*, 1983]. In accordance with the complementary relationship the sum of the computed ET_p and the precipitation was taken to be twice ET_w.

In implementing the AA and CRAE models on a monthly basis, the ground heat flux G is neglected, and ET_a is calculated as a residual of (1).

3. Methodology

Monthly evapotranspiration was estimated for the conterminous United States using the CRAE and AA models. Model estimates were then compared with evapotranspiration estimates for selected basins computed from water balances. On the basis of the record lengths of the available data sets the study was confined to the water years 1962–1988.

3.1. Model Data Sets and Spatial Interpolation

The main advantage of complementary relationship models is that they rely solely on routine climatological observations. Local temperature and humidity gradients in the atmospheric boundary layer respond to, and obviate the necessity for information regarding, the conditions of moisture availability at the surface. The models bypass the complex and poorly understood soil-plant processes and thus do not require data on soil moisture, stomatal resistance properties of the vegetation, or any other aridity measures. Neither do they require local calibration of parameters beyond those built into the models.

The models require data on average temperature, wind speed, solar radiation, humidity, albedo, and elevation. The meteorological input data sets are in discrete format, i.e., point values at station locations. In order to generate estimates of areal evapotranspiration a spatial interpolation technique was applied to the point observations of these variables, and evapotranspiration was calculated at each resulting grid cell.

An analysis of the estimation error invoked by various grid cell sizes conducted by *Claessens* [1996] indicated that for cell sizes larger than 10 km the resultant increase in the variance of the distribution of the estimation error is unacceptable, while smaller cell sizes result in excessive additional computational burden with only a relatively minor decrease of the estimation error variance. Thus all spatial interpolation and analysis was conducted at a 10-km cell size.

Kriging was the a priori preference for spatial interpolation of those climatological inputs (i.e., minimum and maximum temperature) whose station networks would support the inherent semivariogram estimation procedure [*Tabios and Salas*, 1985]. Otherwise, an inverse distance weighted (IDW) scheme was used (i.e., for solar radiation, humidity, and wind speed). For each spatial variable, refinements were made to the chosen scheme in order better to describe the spatial estimates of the variables. These refinements are more fully covered in other sources [*Tabios and Salas*, 1985; *Kitanidis*, 1992; *Bras and Rodríguez-Iturbe*, 1993].

The validity of calculating ET_a with interpolated observations of the meteorological variables was tested by comparing the observed relationship between average annual values of precipitation and ET_a derived using a subset of the basins in this analysis with that derived from data obtained directly (i.e., without spatial interpolation) at the meteorological stations. Significance tests on the regression parameters of the resulting relationships indicated that those obtained for the basin subset results were not significantly different from those of the station results, thus validating this approach.

Temperature data were obtained from the National Climate Data Center (NCDC) data set (EarthInfo, NCDC Summary of the Day (TD-3200 computer file), Boulder, Colorado 1998). Average temperature was estimated as the mean of the average monthly maximum and average monthly minimum temperatures. *Claessens* [1996] presented results from cross-validation analysis testing spatial interpolation schemes for temperature and humidity. It was shown that spatial interpolation of average temperature could be improved by incorporating a simple adiabatic adjustment into the interpolation scheme. The adiabatic adjustment consists of three steps: (1) transforming the temperature values to residuals of potential temperature by subtracting the effects due to elevation-dependent adiabatic expansion (9.8°C 1000 m^{-1}), (2) carrying out ordinary kriging across the entire area of study on the transformed data set, and (3) reversing the potential temperature transformation.

Wind speed data were taken from the Solar and Meteorological Surface Observation Network (SAMSON) [*National Oceanic and Atmospheric Administration* (*NOAA*), 1993] and U.S. Environmental Protection Agency Support Center for Regulatory Air Models. The former source contains hourly data on wind speed collected at 217 stations within the conterminous United States. The latter contains data for 29 National Weather Service (NWS) stations in the later years in the record (i.e., 1984–1988). The raw data were interpolated using a simple IDW scheme without a trend surface.

Solar radiation was estimated from the SAMSON [*NOAA*, 1993]. This data set contains both observed solar radiation from first-order weather stations and modeled solar radiation for selected second-order weather stations. There are a total of 215 stations in the conterminous United States. The data record covers the period 1961 through 1990. In order to improve the interpolation of solar radiation the climatological station monthly means were regressed on station latitude, longitude, and elevation taken individually and in all combinations. For all months, trend surfaces were generated, and the solar radiation data were then interpolated using IDW with detrending.

Humidity was estimated from the NCDC data set (EarthInfo, NCDC Surface Airways (TD-3280 computer file), Boulder, Colorado, 1998). This data set contains long-term records of dew point temperature for first- and second-order NWS stations, with 323 stations in the conterminous United States. The data record for most stations starts in 1948 and is updated continuously. The adiabatic adjustment described for the temperature data set was also applied to dew point temperature, with the IDW scheme used for interpolation of the adiabatically adjusted residuals.

Albedo was estimated using an update from the *Gutman* [1988] average monthly albedo surfaces (G. Gutman, personal communication, 1995). This data set contains albedo estimates derived from the advanced very high resolution radiometer, with an original spatial resolution of about 15 km. Elevation was taken from a 30-arc-sec digital elevation model (National Geophysical Data Center).

3.2. Long-Term, Large-Scale Water Balances

Water balances can be used to estimate evapotranspiration only for timescales over which the surface and subsurface storage changes and diversions are zero or known with some degree of certainty. Assuming stationarity conditions for the climatic forcing, the long-term (i.e., climatological), large-scale water balance for an undisturbed basin should lead to negligible net changes in overall basin moisture storage. For a control volume including the ground surface and transpiring canopy and extending to the groundwater aquifer, the long-term, steady state water balance can be expressed as

$$\mathrm{ET}_a^* = P - Y, \tag{15}$$

where P represents basin-wide precipitation and Y represents basin yield, both expressed as depth equivalents. Basin yield Y includes contributions from both surface and groundwater flow and is estimated by the observed streamflow in the manner of *Eagleson* [1978]. Thus a water balance estimate of the long-term average annual evapotranspiration ET_a^* can be obtained from independent data on precipitation and streamflow. ET_a^* can then be compared with the long-term average annual value as obtained from monthly evapotranspiration estimates using the complementary relationship models ($\mathrm{ET}_a^{\mathrm{MODEL}}$) and provides a means to verify the models.

To estimate ET_a^*, streamflow data were taken from *Wallis et al*. [1991] and *Slack and Landwehr* [1992]. These two data sets contain only those basins with little or no regulation and include corrections for missing values and station relocations. Between them they contain data for about 1475 gauging stations. Both data sets cover the water years 1948 through 1988.

Precipitation estimates were taken from the Parameter-elevation Regressions on Independent Slopes Model (PRISM) [*Daly et al*., 1994]. This data set combines climatological and statistical concepts in an objective precipitation interpolation model and currently contains data at a grid cell size of 4 km and a monthly time step for the period 1940–1999. PRISM was selected as it yielded better results (i.e., lower cross-validation bias and absolute error) than kriging techniques [*Daly et al*., 1994] and was assumed to be the best available estimate of precipitation fields, particularly over the complex terrain that dominates large portions of the western United States.

Table 1. Classification of Selected Basins by Size

	Eastern Basin Set		Complete Basin Set	
Basin Area, km^2	HUCs[a]	Basins	HUCs[a]	Basins
<5,000	62	59	75	72
5,000–10,000	46	30	50	33
10,000–20,000	61	18	68	20
20,000–40,000	64	10	64	10
40,000–100,000	21	2	39	3
>100,000	55	1	55	1
Total	309	120	351	139

[a]HUC, hydrologic unit codes.

3.3. Basin Selection

Because the long-term analysis of the water balance components required that basins meet a criterion of minimal anthropogenic impact, only and all basins included in the two streamflow data sets listed above were considered. It was assumed that interbasin and intrabasin diversions and groundwater pumping were insignificant for the selected basins. In addition to having a relatively low level of intrabasin diversion, *Ramírez and Claessens* [1994] concluded, based on two U.S. Geological Survey (USGS) interbasin transfer inventories [*Petsch*, 1985; *Mooty and Jeffcoat*, 1986], that the basins used in this study were only minimally affected by interbasin diversions.

At the time of this study a comprehensive digital data set of USGS-gauged watershed boundaries did not exist; thus the digital delineation of the USGS eight-digit hydrologic unit codes (HUCs) were used, combined with published sizes of gauge drainage areas. Only and all gauges for which the associated HUCs constituted from 85% to 115% of the gauge drainage area were considered, which together with the requirement of minimum impact resulted in the selection of 139 basins containing a total of 351 HUCs and covering approximately 17.4% of the conterminous United States. Table 1 classifies the selected basins by size. The 120 basins to the east of the Continental Divide, containing a total of 309 HUCs, are the primary focus of this study.

3.4. Water Balance Closure Errors

The average annual water balance closure error ε represents the error invoked in closing a large-scale, long-term water balance using $\mathrm{ET}_a^{\mathrm{MODEL}}$ and is henceforth referred to as the "closure error." Here ε is calculated for each basin, as a percentage of average annual precipitation, from

$$\varepsilon^{\mathrm{MODEL}} = \frac{\sum_{i=1}^{27} \sum_{j=1}^{12} \left(\mathrm{ET}_{a(i,j)}^{\mathrm{MODEL}} - \mathrm{ET}_{a(i,j)}^{*}\right)}{\sum_{i=1}^{27} \sum_{j=1}^{12} P_{(i,j)}} \, 100\%, \tag{16}$$

where i and j are the water year and month, respectively.

Nonzero water balance closure errors must first be considered to be either an overestimation (positive closure error) or underestimation (negative closure error) of evapotranspiration by the models. Other possible explanations, however, which were not quantified in this study, are (1) violations of the assumption of undisturbed conditions, through the effects of groundwater pumping and/or surface water diversions, which were minimized for the gauged basins by the selection criteria; (2) violations of the assumption of negligible net groundwater flow out of the basin; (3) violations of the assumption of stationarity in climatological forcing; (4) errors in the hydroclimatological record; and (5) errors induced by spatial interpolation of the climatic variables.

4. Results

4.1. Spatial Patterns of the Complementary Relationship Components

For the 27 years of record (1962–1988), monthly surfaces were constructed for wind speed, solar radiation, dew point temperature, and average temperature. These surfaces were used as inputs to either the CRAE model or the AA model, or both, resulting in monthly surfaces of ET_p, ET_w, and ET_a. Average annual surfaces of ET_w, ET_p, and ET_a and associated comparative surfaces are presented in Figures 2, 3, and 4, respectively.

Both models predict ET_w with a strong negative latitudinal trend (Figures 2a and 2b), which is a direct result of a similar gradient in the solar radiation-forcing field. However, ET_w^{CRAE} is consistently higher than ET_w^{AA}: The mean excess (Figure 2c), averaged across the entire conterminous United States, is 170 mm yr^{-1}. In calculating ET_w^{CRAE}, the increase in ET_w due to the addition of the b_1 term, which is equivalent to adding 179 mm yr^{-1}, and the upward adjustment of Δp at T_p far outweigh the opposite effect of the correction for back radiation at T_p (i.e., the ΔLW term in (7)). The difference in the radiative terms of the ET_w^{CRAE} and ET_w^{AA} parameterizations resulting from the use of T_p and T_a, respectively, can be expressed as follows (using (6) and (14)):

$$\frac{\Delta_p}{\Delta_p + \gamma} Q_n^* - \frac{\Delta}{\Delta + \gamma} Q_n = \frac{\lambda ET_w^{CRAE} - b_1}{b_2} - \frac{\lambda ET_w^{AA}}{\alpha}. \tag{17}$$

The spatial mean value (averaged across the entire conterminous United States) for this difference (Figure 2d) is found to be only 39 mm yr^{-1} (equivalent to 3 W m^{-2}). The effect of using T_p in the ET_w^{CRAE} parameterization is to increase ET_w^{CRAE} over most of the study area. Generally, the radiative term of the CRAE model adjusted for T_p exceeds the radiative term of the AA model across the area to the east of the Continental Divide, the excess increasing with aridity and decreasing with increasing latitude; the radiative term of the CRAE model adjusted for T_p exceeds that of the AA model in northern Maine and in the northern Great Plains and Great Lakes regions. To the west of the Continental Divide the difference pattern is more heterogeneous, reflecting a strong topographical influence: The Central Valley of California and the Sonoran and Mojave Deserts are all positive (i.e., CRAE term exceeds AA term), while the higher elevations of the western United States (i.e., all significant mountain ranges) are negative (i.e., on the right-hand side of (17) the AA term exceeds CRAE term).

ET_p (Figures 3a and 3b) displays a negative latitudinal gradient similar to ET_w in both models. In the western half of the study area the pattern is complicated by the heterogeneous topography and the decrease in precipitation, resulting in a limitation of moisture supply and subsequent decrease in ET_a and increase in ET_p. Figures 3a and 3b compare the ET_p estimates to observations of class A pan evaporation estimates (ET_p^{PAN}) from 1931 to 1960 interpolated across the conterminous United States as independent estimates of ET_p [*U.S. Geological Survey*, 1970]. While the general spatial patterns of both models are broadly similar to the ET_p^{PAN} map, the pan values are more closely mimicked by ET_p^{CRAE}. The maximum ET_p values occur in the desert Southwest, with a maximum ET_p^{CRAE} of around 3000 mm yr^{-1} in the Imperial and Death Valleys of southwest California and the Sonoran Desert of southern Arizona (peaking at 3046 mm yr^{-1} in Death Valley) and maximum ET_p^{PAN} (>1440 mm yr^{-1}) across southwest California. ET_p^{PAN} slightly exceeds ET_p^{CRAE} (by about 100 mm yr^{-1}) in the High Plains region of the Texas Panhandle, western Oklahoma, Kansas, and southern Nebraska. ET_p^{CRAE} exceeds ET_p^{PAN} (by about 100 mm yr^{-1}) in the Southeast (northern Florida, Georgia, South Carolina, Arkansas, and the southern portions of Mississippi, Alabama, and Louisiana), in Illinois, western Indiana, northern Kentucky, southern Pennsylvania, and in northern New England.

The ET_p^{AA} estimates are very similar to the ET_p^{PAN} estimates across the eastern half and the northern tier of the United States. In the Southwest, ET_p^{PAN} exceeds ET_p^{AA} by about 500 mm yr^{-1}, although the spatial patterns are similar: Both ET_p^{AA} and ET_p^{PAN} attain maximum values in western Texas, southern Arizona, and southwestern California. Both predict lower ET_p with increasing elevation and have lobes of highest ET_p across the Southwest from the Central Valley of California through southern portions of Nevada and Arizona, New Mexico, and western portions of Texas, Oklahoma, and Kansas.

A surface representing the $ET_p^{CRAE} - ET_p^{AA}$ difference (Figure 3c) indicates that ET_p^{CRAE} is consistently and significantly higher than ET_p^{AA}; the mean excess is 199 mm yr^{-1}. The region of greatest excess is, similar to the ET_w results, the desert Southwest, where the excess is of the order of 400–725 mm yr^{-1}. It is only in isolated pockets, northern Texas, southwestern Kansas, southeastern Minnesota, Long Island, and Cape Cod, that ET_p^{AA} exceeds ET_p^{CRAE}; here the excess is 0–120 mm yr^{-1}.

Comparison of the ET_p surfaces suggests a potential difficulty with the wind field input to ET_p^{AA}. Because of the simplicity of the IDW interpolation scheme as applied to U_2, the wind surfaces are very station-oriented, inasmuch as stations with extreme values affect their surrounding regions disproportionately. This leads to higher ET_p^{AA} values around stations with extremely high U_2 estimates, and vice versa. This effect is most pronounced in the eastern half of the study area; in the western half the effect is generally confused by the multifarious effects of the heterogeneous topography on the other variables.

Both models predict the highest values of ET_a (Figure 4a and 4b) around the coastline of the Gulf of Mexico, particularly in southern Florida. ET_a decreases north and west away from the gulf. In the western United States the patterns reflect the complex topography, with local maximum ET_a values observed over higher ground, particularly the Sierra Nevada and Rocky Mountains. The lowest values are in the desert south-

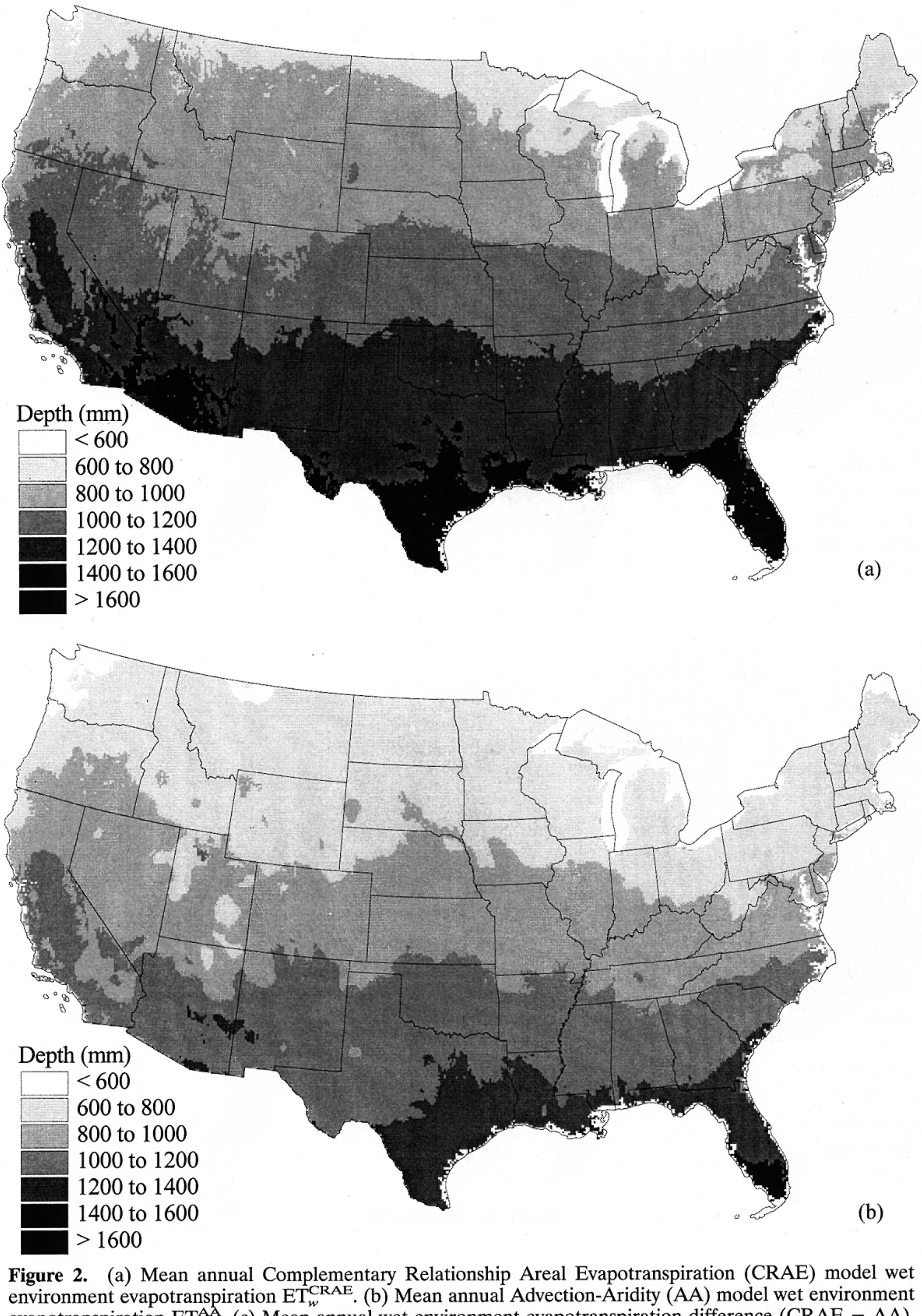

Figure 2. (a) Mean annual Complementary Relationship Areal Evapotranspiration (CRAE) model wet environment evapotranspiration ET_w^{CRAE}. (b) Mean annual Advection-Aridity (AA) model wet environment evapotranspiration ET_w^{AA}. (c) Mean annual wet environment evapotranspiration difference (CRAE − AA). (d) Mean annual difference between T_p and T_a parameterizations of ET_w (i.e., left-hand side of equation (17), CRAE − AA).

west: the Sonoran Desert in southern parts of California, Arizona, and Nevada for the CRAE model and southern parts of California and Nevada for the AA model.

Figure 4c, which shows the $ET_a^{CRAE} - ET_a^{AA}$ difference, indicates that ET_a^{CRAE} exceeds ET_a^{AA} over the entire eastern United States, with the exception of isolated areas in the southeast. The areas of greatest excess of ET_a^{CRAE} over ET_a^{AA} occur in the central Great Plains, south Texas, and south Florida.

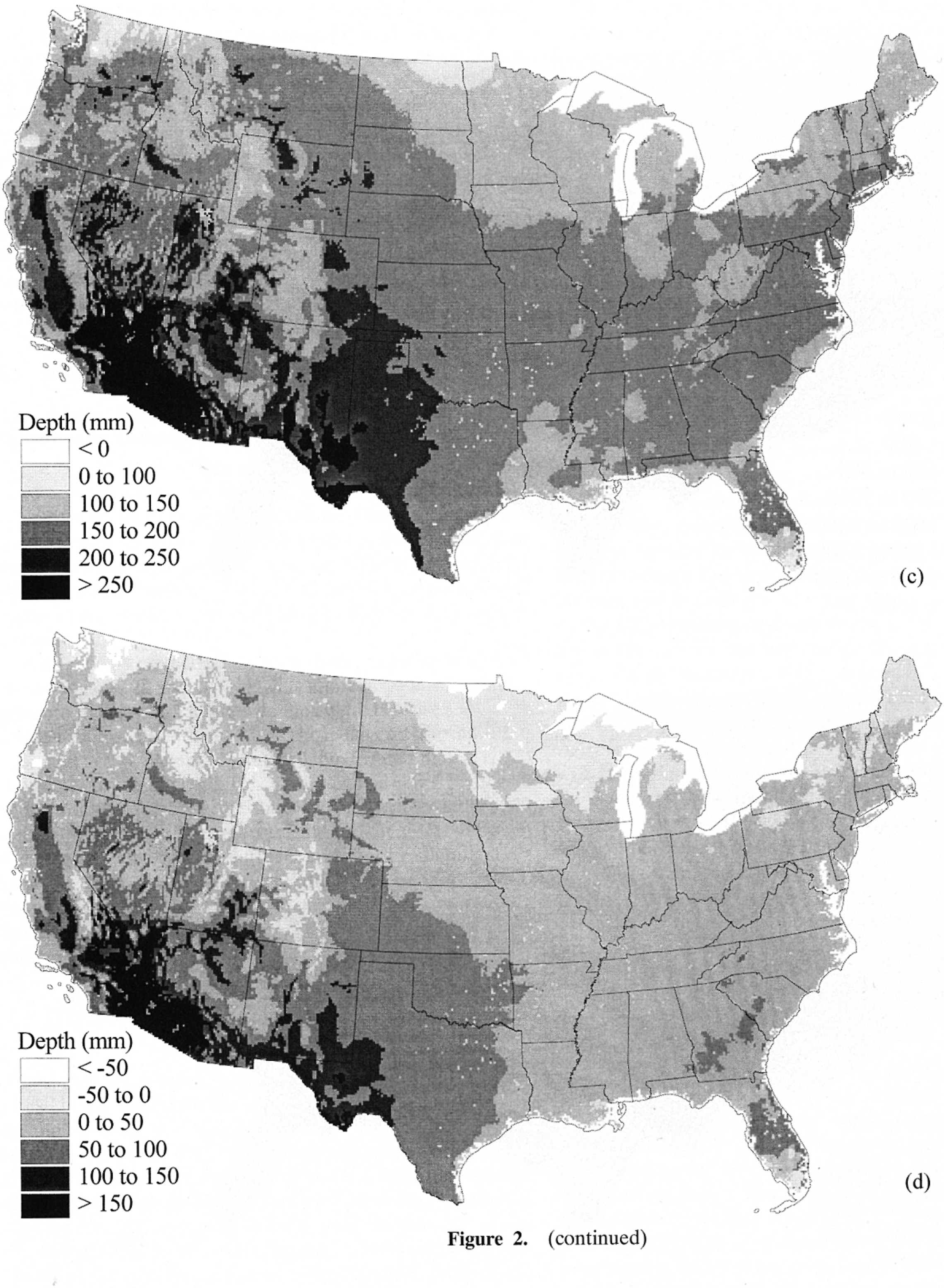

Figure 2. (continued)

Throughout the most arid areas of the west, ET_a^{AA} exceeds ET_a^{CRAE}.

Figures 5a and 5b present average annual surfaces of the difference between precipitation and ET_a^{MODEL} expressed as an average annual depth. This difference represents the average annual yield and includes the effects of contributions from surface runoff, interflow, and groundwater discharge/recharge. Estimates of basin yield are essential products of any evapotranspiration model. For this reason, and because such surfaces facilitate comparison with reports from other evapotranspiration models, they are included here. Generally, yields appear to decrease in a westerly direction as a result of the effects of elevation and aridity on ET_a^{MODEL} and precipitation. For both models, predicted ET_a exceeds precipitation in many areas, indicating overestimation by the evapotranspiration models, underestimation of precipitation by the PRISM

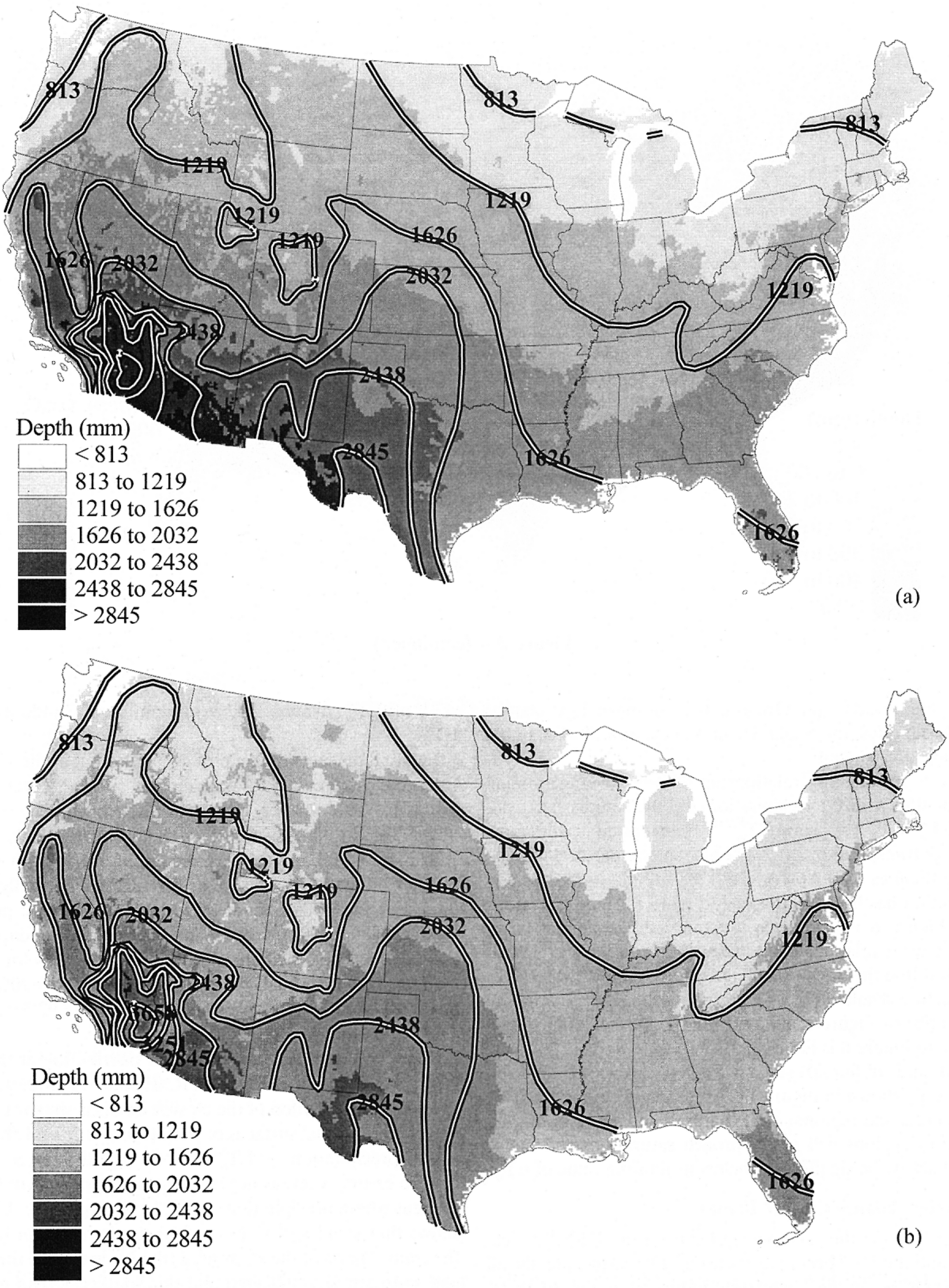

Figure 3. (a) Mean annual CRAE potential evapotranspiration ET_p^{CRAE} (matched to ET_{pan} contours). (b) Mean annual AA potential evapotranspiration ET_p^{AA} (matched to ET_{pan} contours). (c) Mean annual potential evapotranspiration difference (CRAE − AA).

model, or violations of the water balance assumptions (e.g., groundwater depletion, surface water diversions into or from the area, or nonstationarity in climatological forcing). These areas are predominantly to the west of the Great Plains. For the CRAE model, negative yields occur over southern Texas, the High Plains, North and South Dakota, the Basin and Range country of Nevada and Oregon, the southern and central Rocky Mountains, the Snake River Valley, and the Columbia Plateau. The AA model predicts negative yields over a smaller area including southern Texas, the Basin and Range

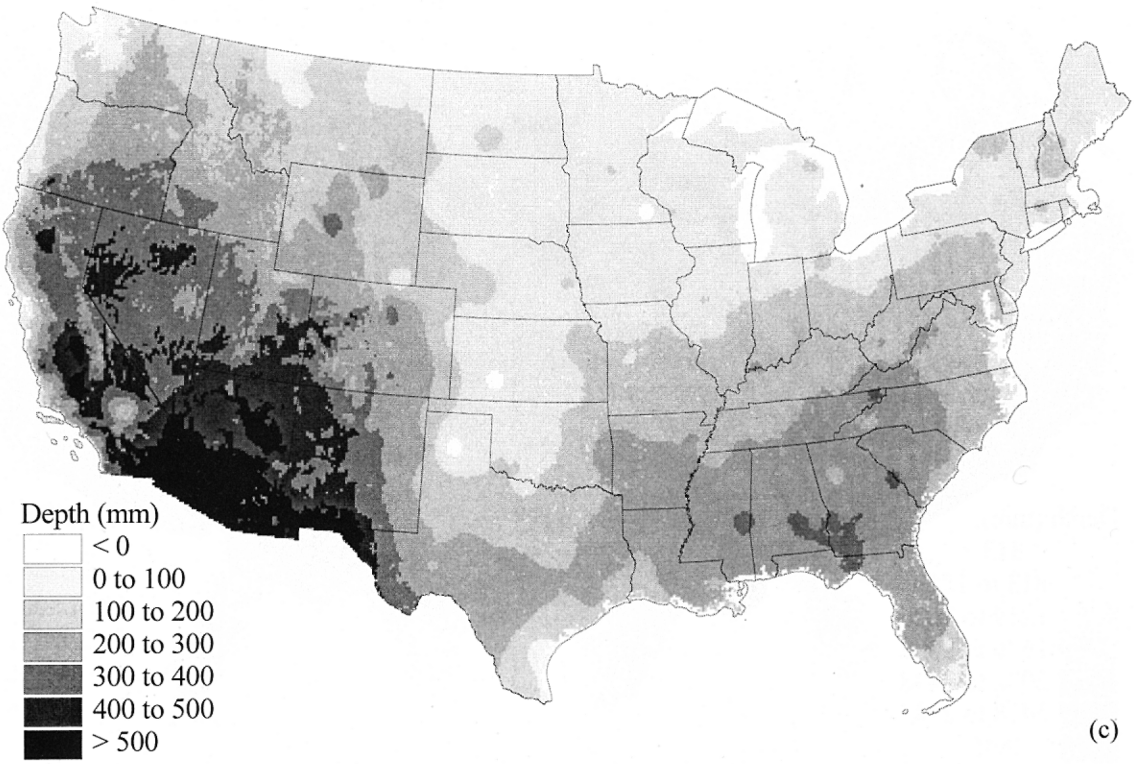

Figure 3. (continued)

country of Nevada and Oregon, the southern and central Rocky Mountains, the Snake River Valley, and the Columbia and Colorado Plateaus.

Figure 6 presents the relationship between average annual values of standardized precipitation and the standardized values of ET_a^*, ET_p^{MODEL}, and ET_w^{MODEL} generated in this study. The evapotranspiration rates have been standardized by expressing them as a fraction of ET_w^{MODEL}. Standardized annual precipitation has been used as a surrogate for moisture availability. Figure 6 indicates that on an average annual basis, there is a clear relationship between ET_a^* and moisture availability and that this is complementary to the one between ET_p and moisture availability, as conceptualized in Figure 1. The resemblance of Figure 1, the theoretical complementary relationship, to Figure 6 is limited to the area to the left (i.e., arid, semiarid, and subhumid) side of the convergence of ET_a and ET_p on ET_w shown in Figure 1. This results from the fact that on an annual and regional basis, natural land surfaces in even the wettest regions will not approach saturation, and hence ET_a will always be significantly below its limiting value of ET_w.

4.2. Water Balance Closure Errors

Figure 7 shows the relationship between the ET_a^{MODEL} estimates and the ET_a^* observations for all 139 basins. Ideally, all points would lie on the 1:1 relation indicated on the graph or, more realistically, would be normally distributed around it with a low variance. For the 120 basins to the east of the Continental Divide, which are the primary focus of this paper, ET_a^{MODEL} is significantly related to ET_a^* ($R^2 = 0.89$ and $p < 0.05$ for CRAE slope; $R^2 = 0.87$ and $p < 0.05$ for AA slope). For the east the greatest divergence between ET_a^{CRAE} and ET_a^* occurs for basins where ET_a^* is under 500 mm yr^{-1}. In these cases, ET_a^{CRAE} overestimates ET_a^*. Substantial divergence between ET_a^{AA} and ET_a^* occurs below about 800 mm yr^{-1} of ET_a^*, where ET_a^{AA} predominantly underestimates ET_a^*.

Figure 8 presents the empirical distribution of the 139 water balance closure errors for both models. Summary statistics are listed in Table 2. The ranges are approximately −25% to +20% for the CRAE model, with one high outlier, and are −30% to +15% for the AA model, with five high outliers. Neither model yields closure errors that are normally distributed. For the CRAE model the closure errors are positively skewed ($\gamma = 0.9908$), with mean +2.35% and standard deviation 7.69%. The distribution of the closure errors for the AA model appears bimodal, with modes at −5% and −20%, and is positively skewed ($\gamma = 1.7501$), with mean −7.92% and standard deviation 12.67%.

Figures 9a and 9b show the spatial distribution of the water balance closure errors for the CRAE and AA models, respectively. The distribution of the closure errors is similar to that of the average annual surfaces of yield (Figures 5a and 5b). Areas where precipitation − ET_a^{MODEL} is negative force positive closure errors, whereas negative closure errors are only found in areas where precipitation − ET_a^{MODEL} is positive. Figure 9a shows that small ε^{CRAE} (+/− 5%) predominate in basins in the central parts of the study area (the Midwest and the central and southern Great Plains) and the Southeast. The more extreme closure errors occur in the western half of the study area, with negative closure errors in the desert Southwest and positive closure errors in New England, the northern Great Plains, southern Texas, and particularly the Basin and Range country of Nevada, Oregon, and Utah.

The ε^{AA} (Figure 9b) are small (+/− 5%) in the Southeast, New England, southern Texas, and isolated basins in North Dakota and the northern Great Lakes region, which are all areas of low elevation or proximity to the ocean. Broadly

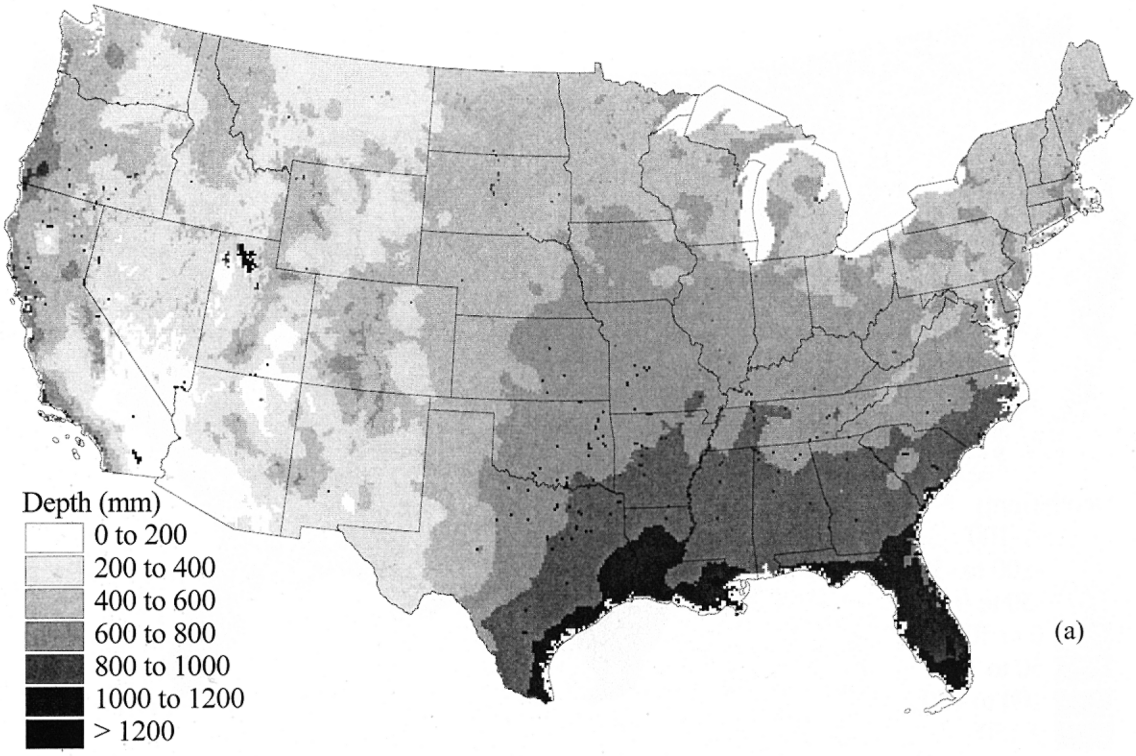

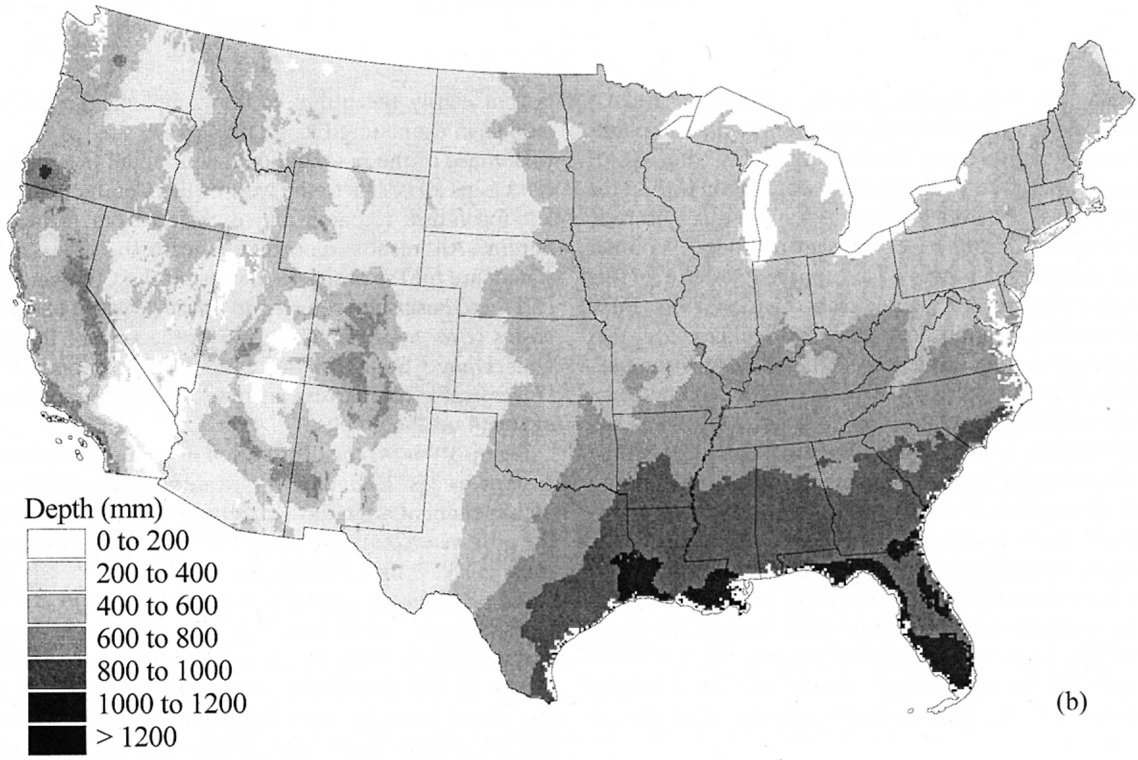

Figure 4. (a) Mean annual CRAE actual evapotranspiration ET_a^{CRAE}. (b) Mean annual AA actual evapotranspiration ET_a^{AA}. (c) Mean annual actual evapotranspiration difference (CRAE − AA).

speaking, negative closure errors are limited to the area to the east of the Continental Divide, and positive closure errors are limited to the mountainous areas surrounding, and to the west of, the divide. Exceptions are few: The basins in the Rio Grande valley and isolated basins in southern Texas, the lower Mississippi valley, the central Appalachians, and the Upper Peninsula of Michigan display positive closure errors, and isolated basins in the Columbia River valley in Washington state, the Basin and Range country in southern Nevada, and in southern Arizona and New Mexico display negative closure errors.

With both models, areas to the west of the Continental

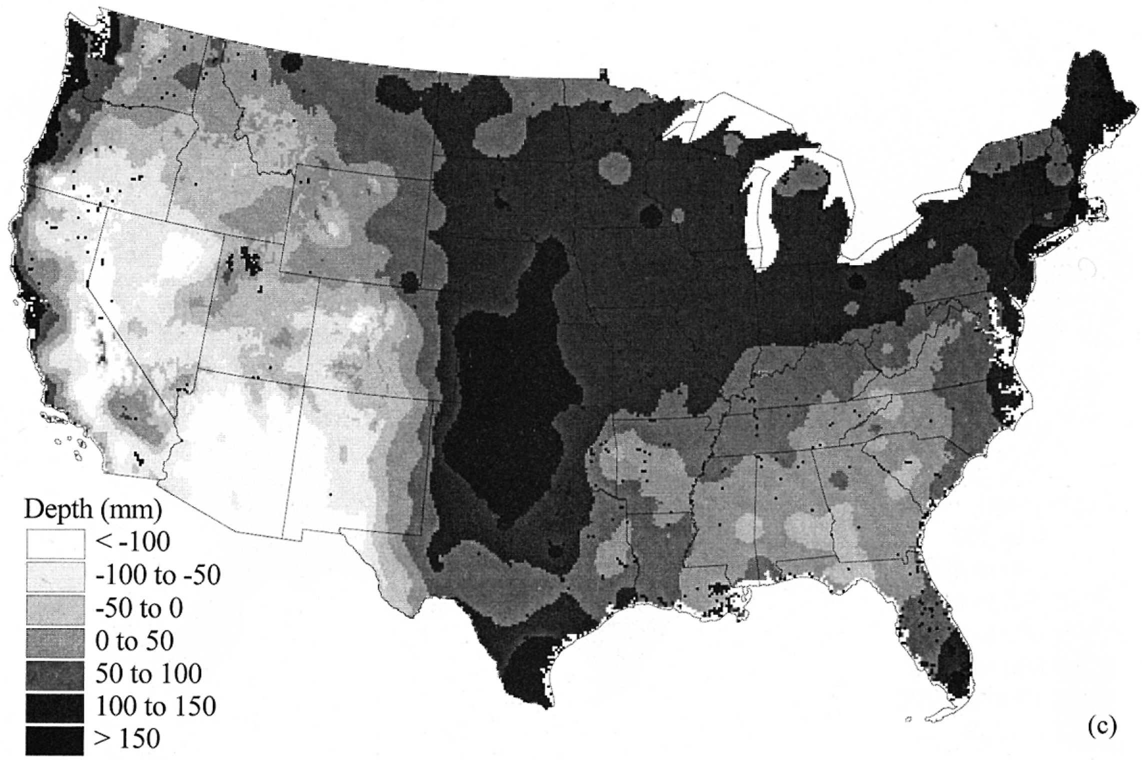

Figure 4. (continued)

Divide display the worst results. The one CRAE and five AA high outliers mentioned previously represent high, arid basins in the desert Southwest and Rocky Mountains (the CRAE outlier and one of the AA outliers represent a basin high in the Rocky Mountains of Colorado, three AA outlier basins are in eastern Arizona and western New Mexico, and one AA outlier basin is in northern Nevada). The apparent failure of the models in these basins may be due to two basic factors. First, the complementary relationship assumes a boundary layer that reflects thorough mixing of the effects of surface environmental discontinuities [*Bouchet*, 1963]. Such mixing occurs over length scales of the order of 100–1000 m [*Bouchet*, 1963; *Davenport and Hudson*, 1967] and is ultimately dependent on the scale of discontinuity and the prevailing atmospheric conditions. The assumption of a well-mixed boundary layer is suspect in many areas to the west of the Continental Divide, where surface heterogeneities abound. The CRAE model, at least, has been shown [*Claessens*, 1996] to perform poorly in areas of high elevation and complex relief. Second, the interpolation of the input variables for estimating the ET_a^{MODEL} and precipitation are increasingly suspect in areas of heterogeneous relief and may lead to significant basin-wide closure errors.

Although the basins in the Pacific Northwest are also in high, rugged terrain, they show better results than do the outlier basins. Large errors in application of the complementary relation are unlikely to be found in more humid basins such as these, where, as shown in Figure 1, the estimates of ET_a are closer to those of ET_p. Hence not only do these basins potentially defy the assumption of a well-mixed boundary layer, but the effects of any misapplication of the complementary relationship here will be obscured by the mitigating effects of greater humidity. It can therefore be assumed that these basins do not clarify the utility of the complementary relationship models in estimating ET_a.

Because of the potential data and model problems in western basins all basins to the west of the Continental Divide are left for future research and excluded from further analysis herein: All results reported henceforth, unless otherwise stated, are for the basins to the east of the Continental Divide, and these basins are referred to as the "eastern basins." These basins cover approximately 21% of the area of the conterminous United States to the east of the Continental Divide. However, for comparison purposes the western basins are still included on the graphs.

Figure 10 shows the distribution of closure errors for the 120 eastern basins. Excluding the western basins from the distribution eliminates the most extreme closure errors (particularly the positive errors). The mean ε^{CRAE} is slightly increased (i.e., from +2.35% to +2.51%), the minimum ε^{CRAE} is increased from −24.87% to −10.67%, and the maximum ε^{CRAE} is decreased from +43.13% to +22.85%. As shown in the histograms (Figures 4 and 5) and reflected in the skewness values (Table 2), the distribution of CRAE closure errors becomes less biased toward positive values ($\gamma = 0.8153$). The effect on the AA closure error set is to decrease the mean ε^{AA} from −7.92% to −10.59% and to decrease the maximum ε^{AA} from +48.71% to +9.70%, leaving the AA distribution more symmetrically distributed around its mean than before. Although the AA distribution appears to be bimodal, with modes at −5% and −15%, the skewness (or g statistic in the skewness test) value of $\gamma = 0.1179$ falls within the bounds of normality at the 5% significance level. Thus the hypothesis of normality cannot be rejected for this distribution.

Figures 11a through 11c depict the effects of basin climatology upon the performance of the models, as measured by the

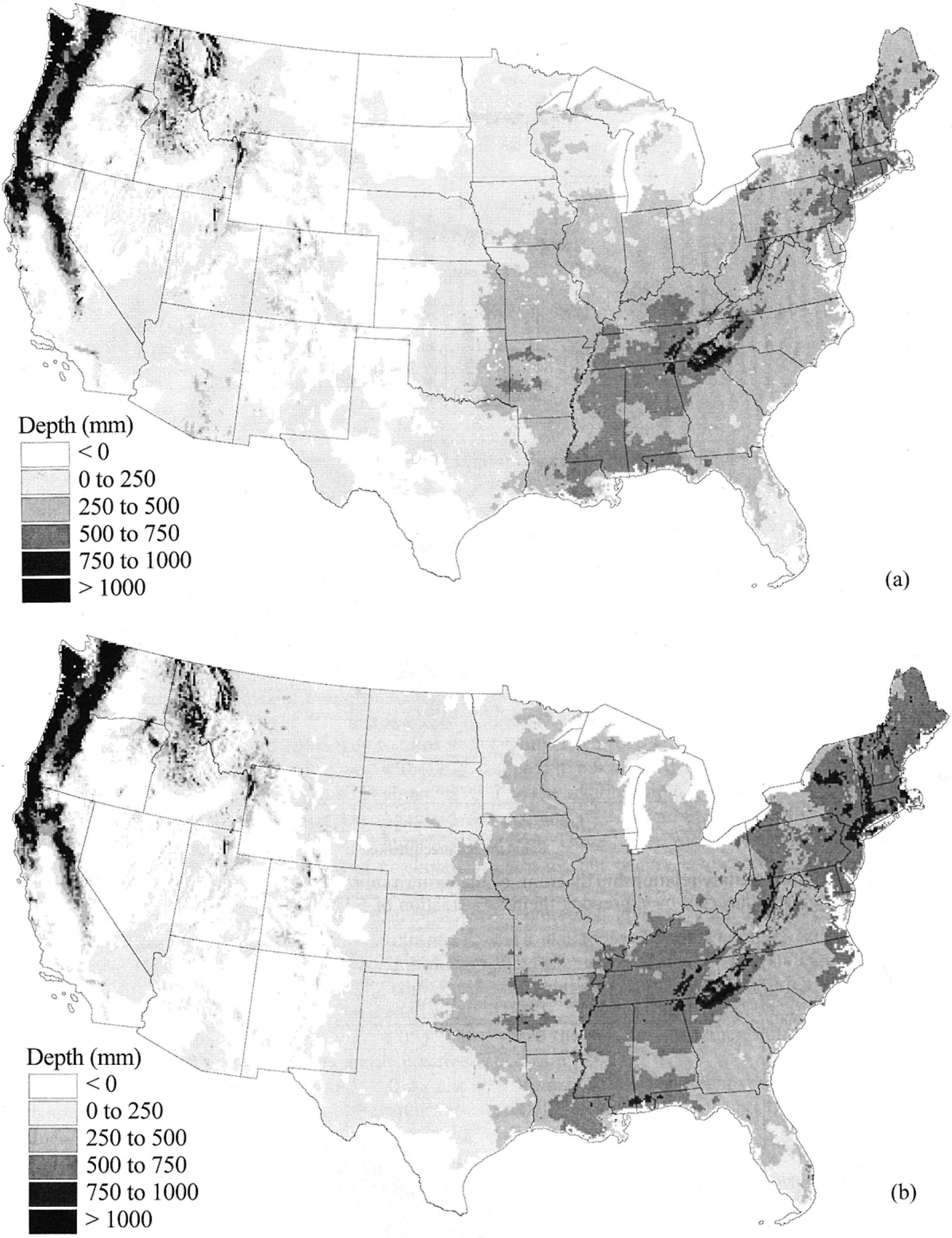

Figure 5. (a) Mean annual CRAE yield. (b) Mean annual AA yield.

water balance closure errors $\varepsilon^{\mathrm{CRAE}}$ and $\varepsilon^{\mathrm{AA}}$. Each of the dependent variables, average annual precipitation (Figure 11a), average annual precipitation minus streamflow (Figure 11b), and average annual relative evapotranspiration ($\mathrm{ET}_a^{\mathrm{MODEL}}/\mathrm{ET}_p^{\mathrm{MODEL}}$) (Figure 11c), is a measure of moisture availability (i.e., aridity or humidity) of the basin, with aridity increasing toward the left in each graph. To some degree these aridity measures may be considered surrogates of the degree of continentality of the basins.

Figure 11a relates closure error to mean annual basin-wide precipitation. For the sake of clarity the independent variable is shown up to 1600 mm only; an outlier at 3000 mm is not shown, but it does not affect the regression results. The $\varepsilon^{\mathrm{CRAE}}$ decrease with precipitation ($R^2 = 0.15$ and $p < 0.05$),

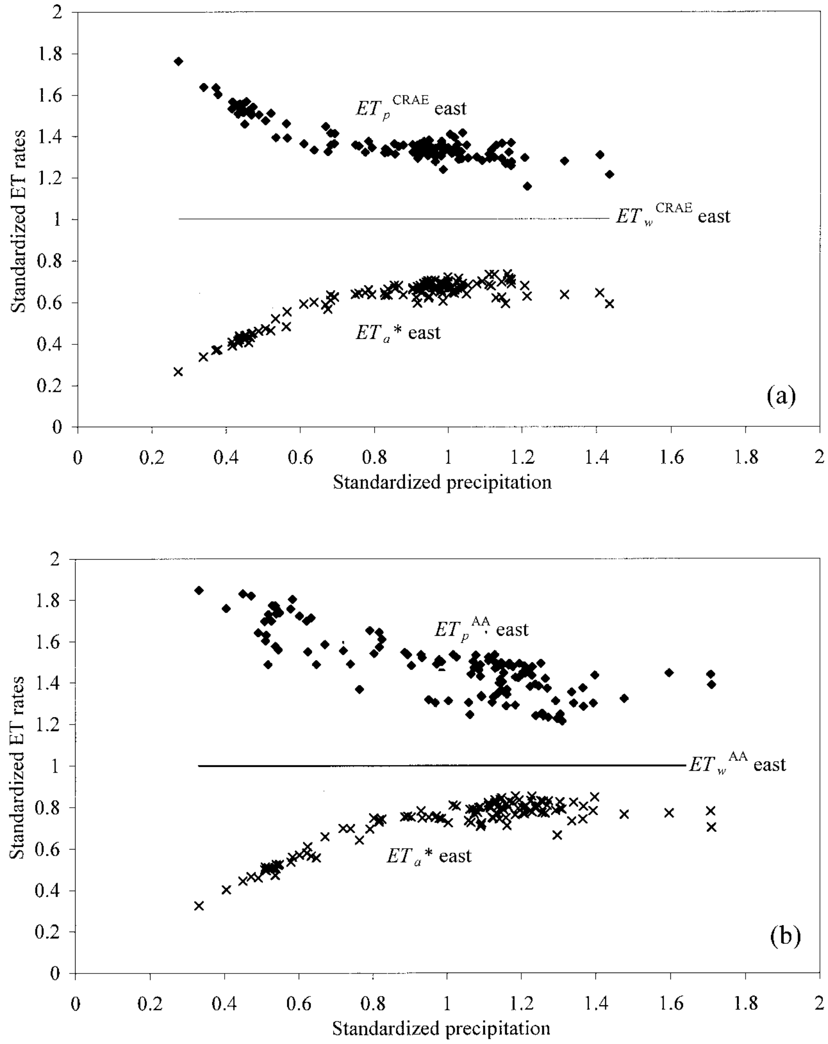

Figure 6. Complementary relationship diagrams of the eastern subset: (a) CRAE model and (b) AA model. Rates have been standardized by expressing them as a fraction of ET_w^{MODEL}.

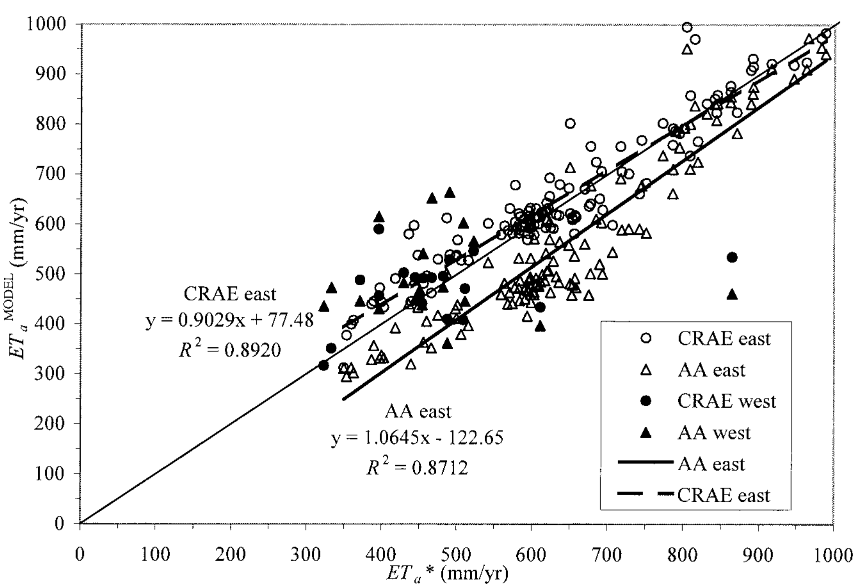

Figure 7. ET_a^{MODEL} versus ET_a^*.

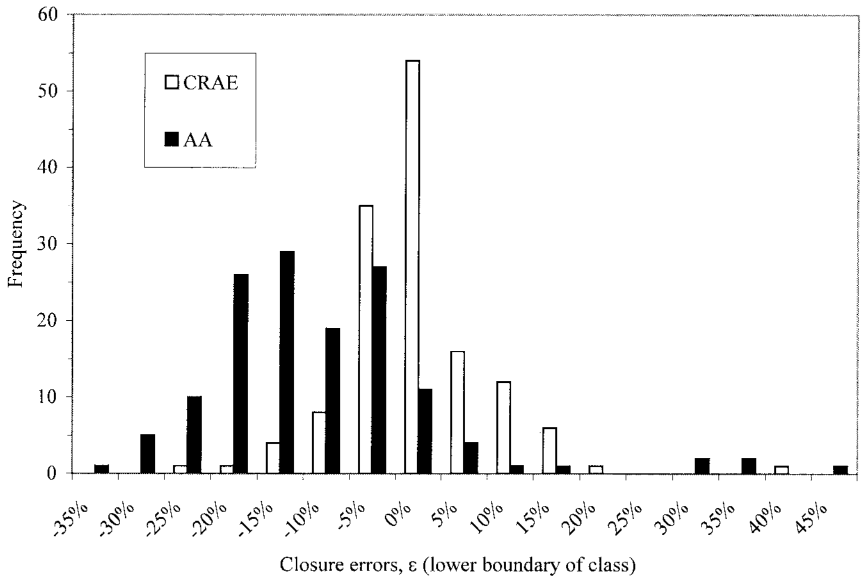

Figure 8. Histogram of closure errors ε^{CRAE} and ε^{AA} of the complete basin set.

tending toward zero at approximately 1200 mm yr^{-1}. The ε^{AA} increases with precipitation ($R^2 = 0.31$ and $p < 0.05$), tending toward zero at about 1400 mm yr^{-1}. Thus the predictive powers of both models increase with humidity.

These trends are also evident in the relationship between ε^{MODEL} and the independent estimates of evapotranspiration ET_a^*, provided by (15) (Figure 11b). The ε^{CRAE} decreases with ET_a^* ($R^2 = 0.18$ and $p < 0.05$) and converges to zero at approximately 800 mm yr^{-1}. The ε^{AA} increases with ET_a^* ($R^2 = 0.18$ and $p < 0.05$) and converges to zero at about 900 mm yr^{-1}. The scatter of ε^{AA} increases with aridity. Again, for both models the ET_a^{MODEL} estimate improves with humidity.

The effect of the relative degree of soil control or climate control of evapotranspiration (i.e., effect of moisture availability at the land surface) on water balance closure can be assessed by relating the closure error to relative evapotranspiration ET_a/ET_p (Figure 11c). Increasing this ratio is equivalent to moving to the right in Figure 1: ET_a and ET_p converge toward ET_w. The ε^{CRAE} are slightly negatively correlated with relative evapotranspiration ($R^2 = 0.01$ and $p < 0.05$), although very scattered. The ε^{AA} display a consistently positive relationship with relative evapotranspiration ($R^2 = 0.43$ and $p < 0.05$) and converge toward zero; for relative evapotranspiration values below approximately 0.36, there is increased scatter in ε^{AA}. These results indicate that the performance of the CRAE model is nearly independent of the degree of saturation of the basin land surface, whereas ET_a^{AA} estimates improve with increasing basin saturation.

The relationship between the closure errors and the mean annual basin-wide evaporation temperature difference ($T_p - T_a$) is shown in Figure 11d. Note that the range for this temperature difference is approximately +/−2.5°C. The relationship between evaporation temperature difference and ε^{CRAE} is slightly negative ($R^2 = 0.06$ and $p < 0.05$). The ε^{CRAE} appear to be centered around zero for basins where T_p exceeds T_a. The relationship between evaporation temperature difference and ε^{AA} is significantly positive ($R^2 = 0.34$ and $p < 0.05$). The ε^{AA} are widely scattered for basins where T_a exceeds T_p but converge toward zero for basins where T_p exceeds T_a.

Figure 11d indicates that the two ET_a^{MODEL} estimates are most similar for basins where T_p exceeds T_a. This result is somewhat more subtle than that stated by *Morton* [1983, p. 21], who claimed that "the analytical solution of *Penman* [1948] . . . [is] accurate only under relatively humid conditions where the equilibrium temperature [T_p] is near the air temperature [T_a]."

Morton's [1983] statement above and the fact that the CRAE model was calibrated using data from arid basins imply that the CRAE model should significantly outperform the AA model in arid regions. This implication is borne out by examining the closure errors at the arid end of the climatic spectrum. For the

Table 2. Summary Statistics for Water Balance Closure Errors

Statistic	Eastern Basin Set CRAE Model	Eastern Basin Set AA Model	Complete Basin Set CRAE Model	Complete Basin Set AA Model
Mean (percent precipitation)	2.51	−10.59	2.35	−7.92
Median (percent precipitation)	1.22	−11.87	1.24	−10.55
Minimum (percent precipitation)	−10.67	−28.16	−24.87	−30.11
Maximum (percent precipitation)	22.85	9.70	43.13	48.71
Standard deviation (percent precipitation)	6.32	8.09	7.69	12.67
Skewness	0.8153	0.1179	0.9908	1.7501

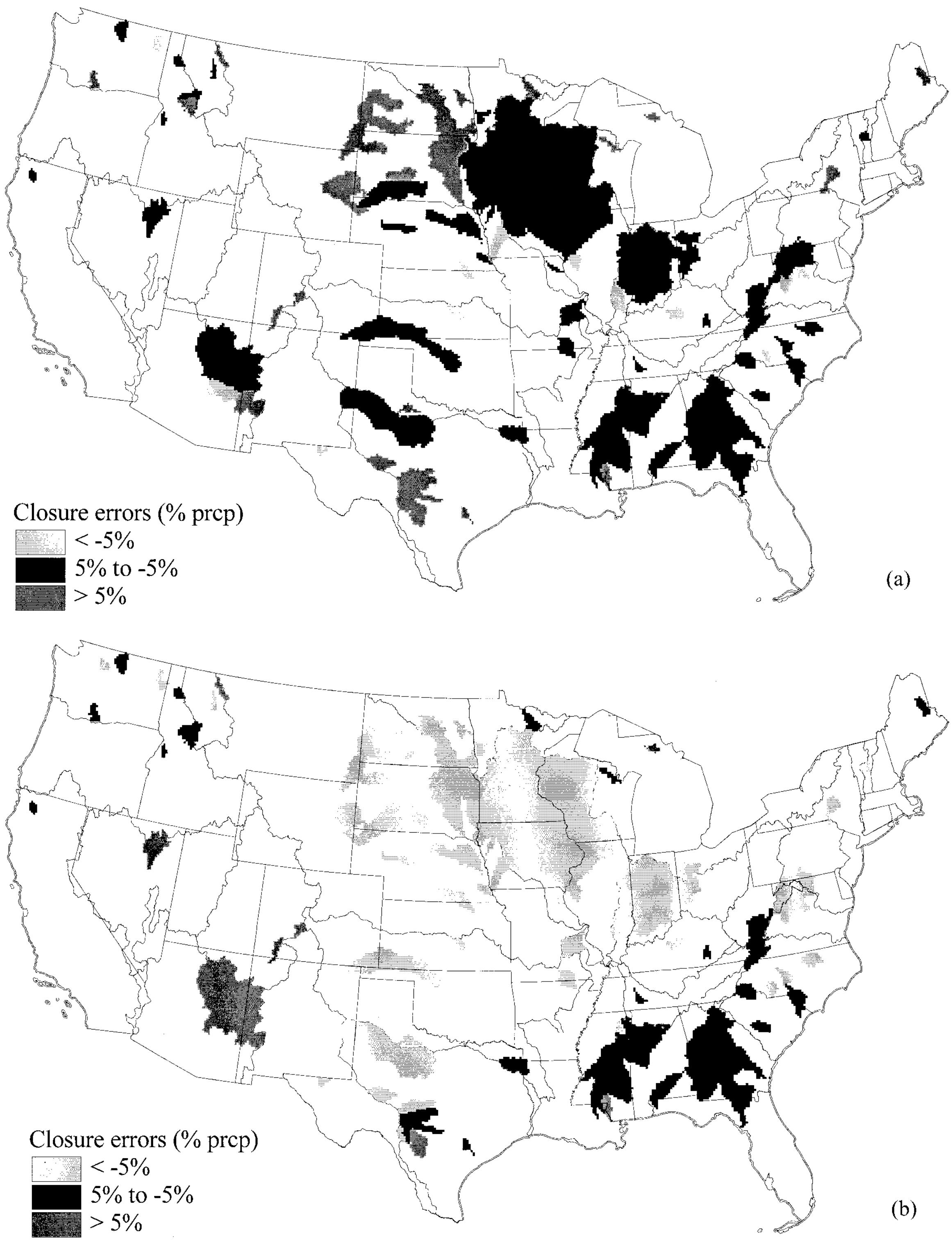

Figure 9. (a) Geographic distribution of CRAE closure errors of the complete basin set. (b) Geographic distribution of AA closure errors of the complete basin set.

cluster of one CRAE and five AA positive outliers the temperatures at which the evaporative processes are evaluated are significantly different (T_a exceeds T_p by 1.5°–2°C), yet for four of the five outliers the CRAE model performs well ($\varepsilon^{\mathrm{CRAE}}$ ranges from $+7.58\%$ to -1.93%).

In the conterminous United States, continental-scale precipitation displays an overall, climatological gradient from a humid climate in the east to a semiarid climate in the west. As continental-scale elevation generally increases similarly in an east-west direction, there is a strong negative correlation between precipitation and elevation, particularly across the study area to the east of the Continental Divide. Thus, when comparing $\varepsilon^{\mathrm{MODEL}}$ with mean basin elevation, one would expect a similar relationship to that observed between closure error and

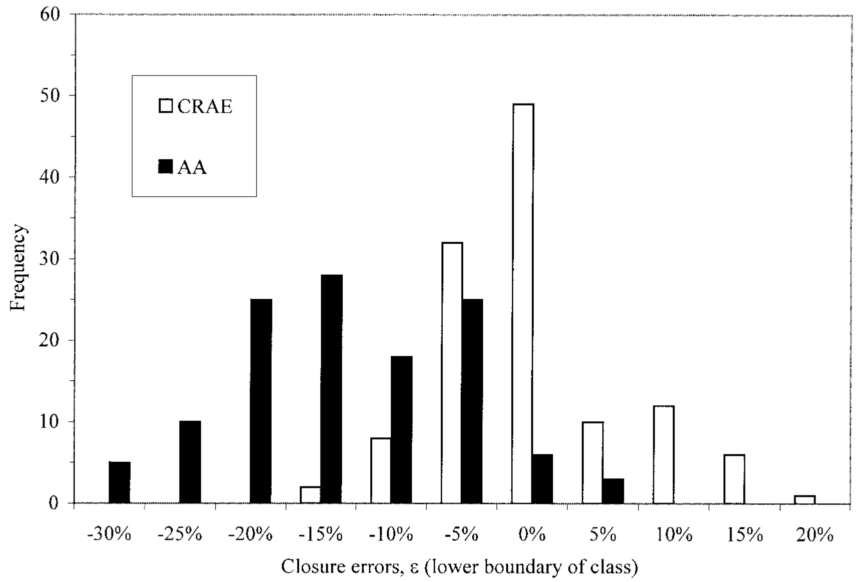

Figure 10. Histogram of closure errors ε^{CRAE} and ε^{AA} of the eastern subset.

average annual basin precipitation (Figure 11a). Figure 12 demonstrates that for the CRAE model, closure errors do indeed increase with elevation ($R^2 = 0.05$ and $p < 0.05$), with ε^{CRAE} tending toward zero for the lowest basins. The ε^{AA} exhibit a strong negative correlation with basin elevations ($R^2 = 0.14$ and $p < 0.05$).

As expected from a misapplication of the complementary relationship in the rugged terrain of the western basins, the set of basins with the highest elevations, and therefore the most rugged terrain, exhibits the most scatter. The cluster of ε^{MODEL} above +30% is for high, arid basins in the desert Southwest and the Rocky Mountains. Of the western basins the highest closure errors ($\varepsilon^{CRAE} = +43.13\%$ and $\varepsilon^{AA} = +48.71\%$) occur at the greatest elevation (2966 m) (Figure 12).

Figure 13 shows the relationship between ε^{MODEL} and mean annual basin wind speed and demonstrates the effects of the different treatments of advection in the two models. The ε^{CRAE} are weakly positively correlated with wind speed ($R^2 = 0.07$ and $p < 0.05$). They are clustered around zero for the lowest wind speeds and increase in variability with increasing wind speed. This near independence of the CRAE model's performance with wind speed appears to support *Morton*'s [1983] treatment of advection. The ε^{AA} are strongly negatively correlated with, and hence the AA model is very sensitive to, wind speed ($R^2 = 0.50$ and $p < 0.05$). In fact, mean annual wind speed exhibits the strongest relationship with ε^{AA} of any climatic variable. This suggests that the first step in improving the AA model should be to reparameterize the wind function $f(U_2)$. This reparameterization is the subject of *Hobbins et al.* [this issue].

The fact that the positive outliers in particular and the western basins in general have wind speeds toward the low end of the range (i.e., <4 m s^{-1}) points to a deficiency in the spatial interpolation of the wind speed data in the mountainous areas, as one would expect to find higher mean annual basin-wide wind speed for the highest, most rugged basins. An attempt was made to improve the interpolation of the wind speed fields by using trend surfaces. For each month, climatological (i.e., across the length of the record) mean wind speed values were generated for each station, and these values were regressed on the station latitude, longitude, and elevation taken individually and in all combinations. However, no distinct trends could be found, and the attempt was abandoned.

5. Summary and Conclusions

Average annual surfaces of ET_w and ET_p indicate gradients that are a result of gradients in radiative forcing and a combination of radiative and precipitation forcing, respectively. The effects of elevation, through precipitation forcing and/or the vapor transfer function parameter f_T, are most evident in the modeled surfaces of ET_p. For both components of the complementary relationship, ET_p and ET_w, the estimates generated by the CRAE model exceed those of the AA model. The resulting modeled ET_a surfaces show a negative latitudinal gradient in the eastern half of the conterminous United States and a positive elevational gradient for western areas. In the western part of the study area, regions were identified where modeled ET_a exceeds precipitation on an average annual basis. For the AA model these areas correspond to the areas of lowest precipitation, whereas for the CRAE model such a correspondence is less evident. These regions of negative yield are generally associated with irrigated agriculture, groundwater depletion, and/or surface water diversions. However, the spatial extent and magnitude of this precipitation deficit could be an indication that the ET_a estimates produced by the models are too high. This can be attributed to either the models themselves or to the inappropriateness of the meteorological forcing fields, either through low data quality or inadequacies involved in their spatial interpolation.

The b_1 term in ET_w^{CRAE}, included to allow for any periods of negative radiation, increases ET_w^{CRAE} by approximately 179 mm yr^{-1}, which almost exactly accounts for the excess of long-term average ET_w^{CRAE} over ET_w^{AA}. If b_1 were neglected, ET_w^{CRAE} would be very close to the standard Priestley-Taylor parameterization used for ET_w^{AA}.

All of the positive AA and CRAE closure errors in the Basin and Range country, the northern Great Plains, and southern Texas are a direct result of the negative yields predicted for

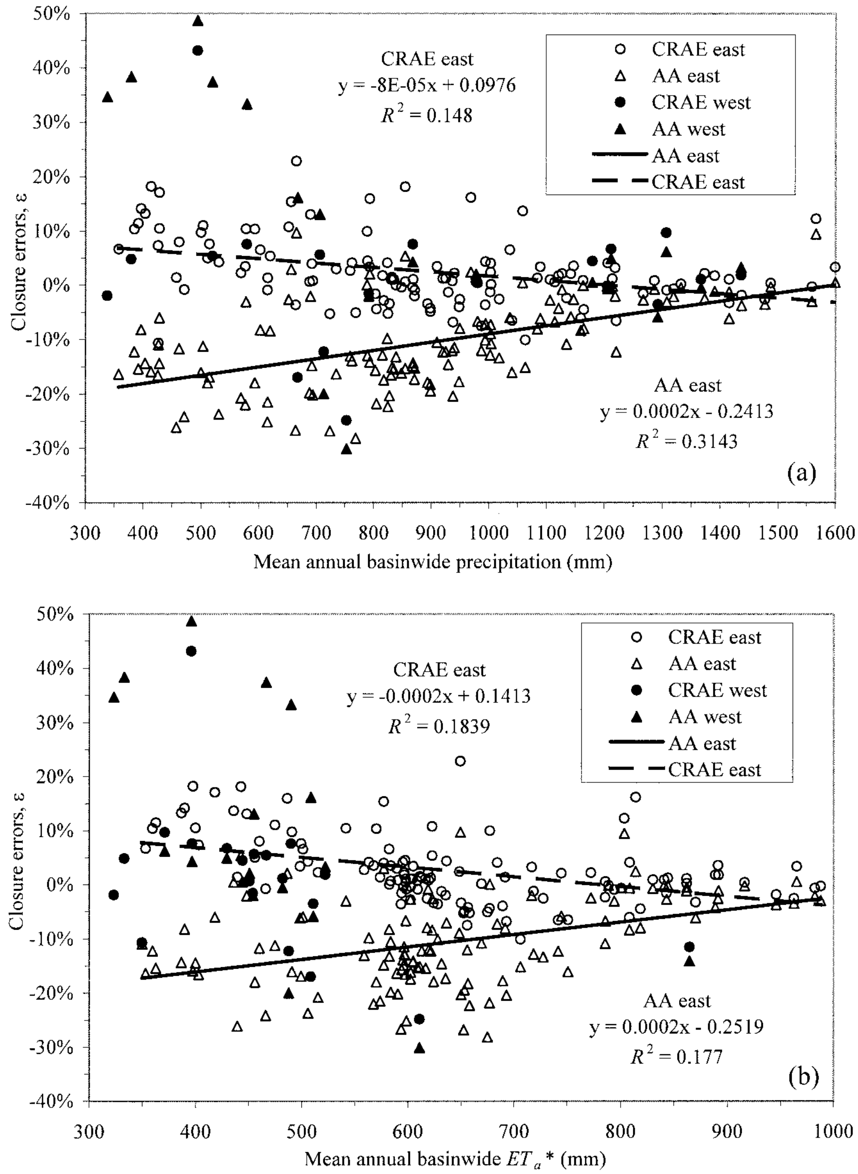

Figure 11. (a) Closure errors versus mean annual basin-wide precipitation. (b) Closure errors versus mean annual basin-wide ET_a^*. (c) Closure errors versus mean annual basin-wide relative ET_a^{MODEL}. (d) Closure errors versus mean annual basin-wide evaporation temperature difference.

these areas. These could result from the effect of irrigated agriculture, through groundwater depletion and surface water diversions, which would be a violation of the assumption of minimum impact. Most other CRAE closure errors are of the order of +/−5% and do not appear spatially biased. Almost all other AA closure errors are negative and may result from a poorly calibrated wind function.

Both models' performances are affected by basin climatology. The CRAE model underestimates ET_a slightly in humid climates and overestimates slightly in arid climates, which supports the conclusions in other work by *Hobbins et al.* [1999] where it was found that the CRAE model performs less well under arid and advective conditions (i.e., that it tends to overestimate ET_a). The AA model generally underestimates ET_a in all but the most extreme arid climates at high elevations. Scatterplots of closure error versus aridity measures (Figures 11a, 11b, and 11c) show that both models yield closure errors that increase in variability with increasing aridity but converge toward zero with increasing humidity. These trends are also reflected in the relationship of the closure errors with mean basin elevation (Figure 12), which in the case of the eastern United States may be considered a surrogate for continentality or aridity.

Moving toward the other end of the climatic spectrum (i.e., increasing moisture availability), the predictive powers of both models increase in moving toward regions of increased climate control of evapotranspiration rates and decrease in moving toward regions of increasing soil control. Increased climate or soil control in this context refers to increased and decreased moisture availability. Because irrigated agriculture is often associated with areas of low moisture availability, these trends could be a direct reflection of anthropogenic influences (i.e., through net groundwater withdrawals and net diversion of surface waters) not sufficiently mitigated against in the basin

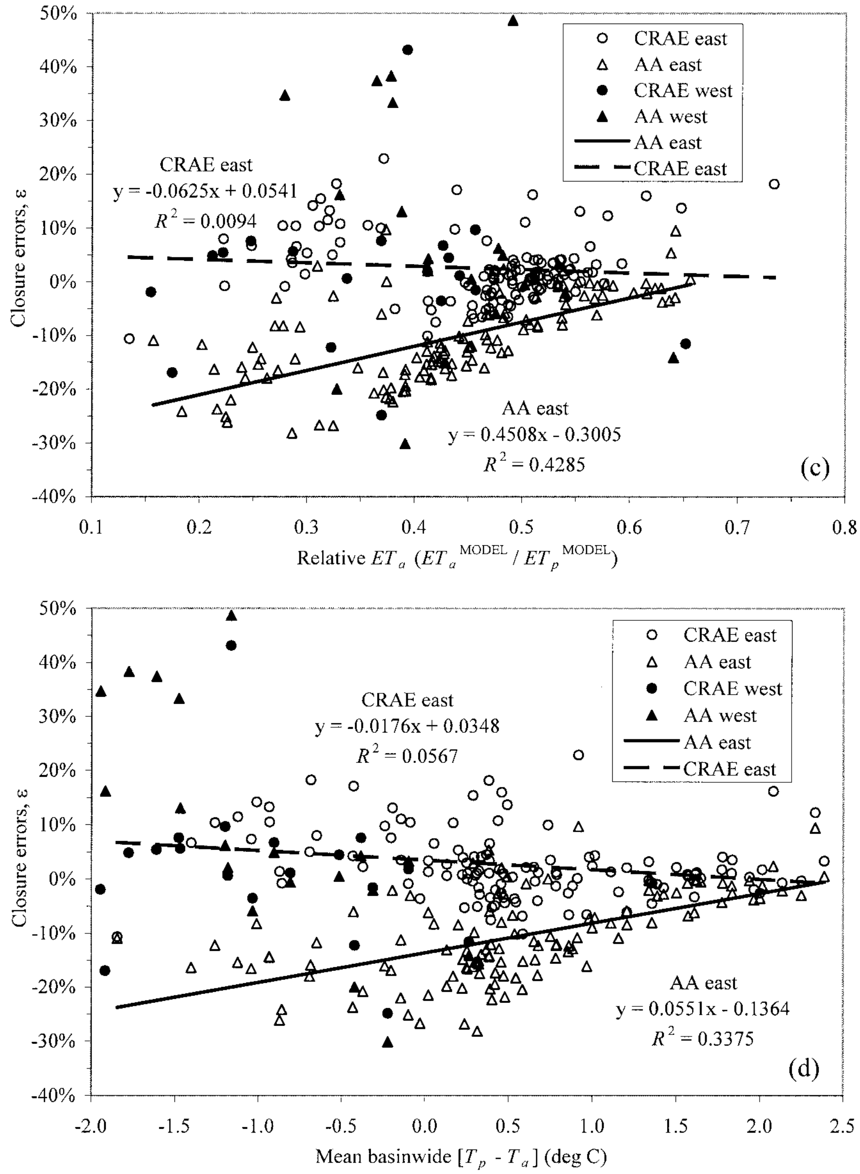

Figure 11. (continued)

selection procedure. However, it should be noted that groundwater pumping in a study basin affects only the independent evapotranspiration estimate ET_a^* not the $\mathrm{ET}_a^{\mathrm{MODEL}}$ estimate. Indeed, one of the primary advantages of complementary relationship models is that the assumption of the integration of atmospheric moisture accounts for all surface hydrology, and therefore their utility is unaffected in basins where groundwater pumping is present.

The models differ significantly in their treatments of the temperature at which the evaporative processes are evaluated. The AA model, in using the Penman equation, uses the air temperature T_a. The CRAE model hypothesizes an equilibrium temperature T_p at which the radiative and vapor transfer components of the evaporative process are equal. The other significant difference between the two models is their treatments of advection. The AA model uses actual wind speed data to calculate the drying power of the air E_a in the expression for $\mathrm{ET}_p^{\mathrm{AA}}$, whereas the CRAE model calculates $\mathrm{ET}_p^{\mathrm{CRAE}}$ by use of a vapor transfer coefficient f_T, independent of wind speed.

The near-zero mean annual CRAE closure error appears to support *Morton*'s [1983] reasoning for using a wind transfer coefficient that is independent of observed wind speeds. However, the positive correlation observed between the CRAE closure errors and climatological basin-wide wind speed, although weak, suggests that there is some opportunity to improve this model's treatment of advection. The elevational effects on $\mathrm{ET}_a^{\mathrm{CRAE}}$ could be better modeled by reparameterizing the vapor transfer function f_T in (11) and reestimating the values of the b_1 and b_2 parameters in the expression for $\mathrm{ET}_w^{\mathrm{CRAE}}$ (14) by another regional calibration in representative arid, mountainous areas.

The strong negative correlation of the AA closure errors with wind speed clearly demonstrates the sensitivity of this model to the wind function $f(U_2)$ described in (4), which was first proposed [*Brutsaert and Stricker*, 1979] for use in the AA model operating at a temporal scale of the order of days. These results highlight the need for a reparameterization of this component of $\mathrm{ET}_p^{\mathrm{AA}}$ to yield both accurate ET_p estimates and

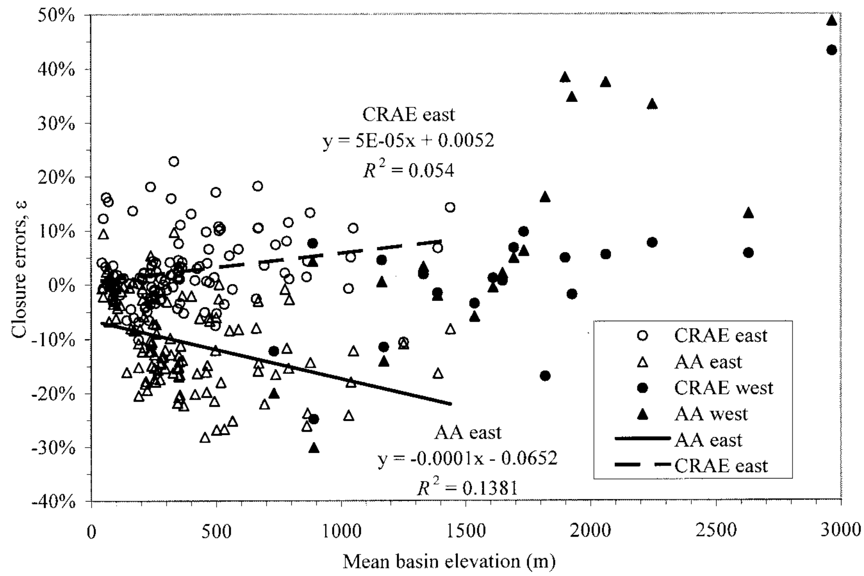

Figure 12. Closure errors versus mean basin elevation.

unbiased water balance estimates on a monthly basis (i.e., a parameterization specific to regional spatial scales and monthly temporal scales). These potential improvements are the subject of *Hobbins et al.* [this issue].

On a mean annual basis the relationships observed between the ET_p^{MODEL} components and the independent estimates of regional evapotranspiration ET_a^* are very similar to the theoretical complementary relationship. Although the performances of both models improve markedly with increasing humidity, it must be noted that in humid basins the ET_a^{MODEL} estimate more closely approaches the ET_p^{MODEL} estimate. Hence the complementary behavior underpinning observation in such basins may not be as apparent.

Although an independent, theoretical proof of the complementary relationship hypothesis has not yet been established, this study provides indirect evidence supporting its plausibility. However, it is important to mention that the observed performance of the models should not only be attributed to their basic, driving hypothesis but also to *Morton*'s [1983] and *Brutsaert and Stricker*'s [1979] choice of governing equations and their applicability at the regional spatial scale and monthly temporal scale. Within this context, *LeDrew*'s [1979, p. 500] statement regarding the CRAE model that "For long-term means its success must depend on calibration procedures . . . and errors which are self-compensating in the long run" should be borne in mind. Overall, the excellent performance of the CRAE model, at least in the eastern United States, demonstrates its utility in providing independent estimates of ET_a in regions across the climatic spectrum, while further enhancing the importance of the concept of the complementary relationship for hydrometeorological applications.

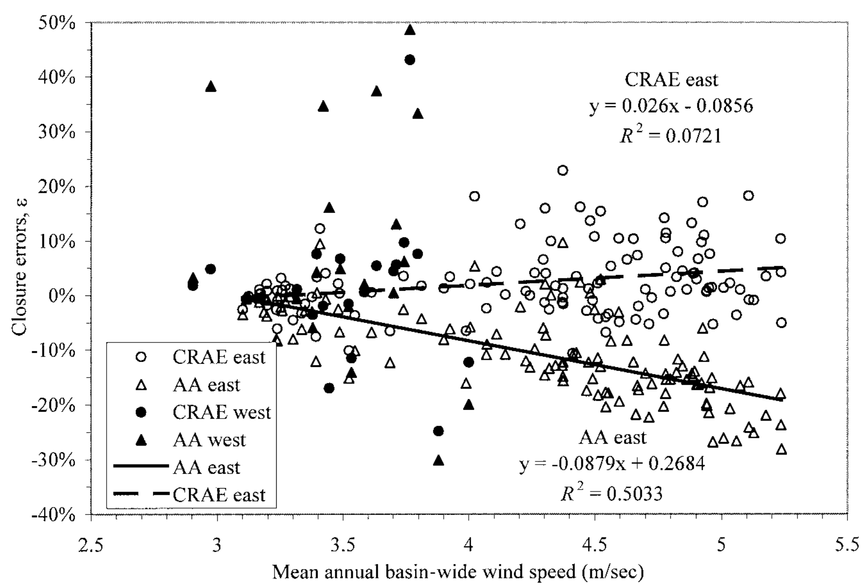

Figure 13. Closure errors versus mean annual basin-wide wind speed.

Acknowledgments. This work was partially supported by the U.S. Forest Service and the National Institute for Global Environmental Change through the U.S. Department of Energy (Cooperative Agreement DE-FC03-90ER61010). In addition, one of the authors (Jorge A. Ramírez) received partial support from the Colorado Water Resources Research Institute. This paper benefited greatly from comments by Guido Salvucci and two other anonymous reviewers.

References

Ben-Asher, J., Estimating evapotranspiration from the Sonoita Creek watershed near Patagonia, Arizona, *Water Resour. Res.*, *17*(4), 901–906, 1981.

Bouchet, R. J., Evapotranspiration réelle evapotranspiration potentielle, signification climatique, Int. Assoc. Sci. Hydrol., Berkeley, Calif., *Symp. Publ. 62*, pp. 134–142, 1963.

Bras, R. L., and I. Rodríguez-Iturbe, *Random Functions and Hydrology*, 559 pp., Dover, Mineola, N. Y., 1993.

Brutsaert, W., and H. Stricker, An advection-aridity approach to estimate actual regional evapotranspiration, *Water Resour. Res.*, *15*(2), 443–450, 1979.

Chiew, F. H. S., and T. A. McMahon, The applicability of Morton's and Penman's evapotranspiration estimates in rainfall-runoff modeling, *Water Resour. Bull.*, *27*(4), 611–620, 1991.

Claessens, L., The complementary relationship in regional evapotranspiration and long-term large-scale water budgets, M.S. thesis, 159 pp., Hydrol. Sci. and Eng. Program, Civ. Eng. Dept., Colo. State Univ., Fort Collins, 1996.

Daly, C., R. P. Neilson, and D. L. Phillips, A statistical-topographic model for mapping climatological precipitation over mountainous terrain, *J. Appl. Meteorol.*, *33*, 140–158, 1994.

Davenport, D. C., and J. P. Hudson, Local advection over crops and fallow, I, Changes in evaporation along a 17-km transect in the Sudan Gezira, *Agric. Meteorol.*, *4*, 339–352, 1967.

Dooge, J. C. I., Hydrologic models and climate change, *J. Geophys. Res.*, *97*(D3), 2677–2686, 1992.

Doyle, P., Modeling catchment evaporation: An objective comparison of the Penman and Morton approaches, *J. Hydrol.*, *12*, 257–276, 1990.

Eagleson, P. S., Climate, soil and vegetation, 7, A derived distribution of annual water yield, *Water Resour. Res.*, *14*(5), 765–776, 1978.

Granger, R. J., A complementary relationship approach for evaporation from nonsaturated surfaces, *J. Hydrol.*, *111*, 31–38, 1989.

Granger, R. J., and D. M. Gray, Examination of Morton's CRAE model for estimating daily evaporation from field-sized areas, *J. Hydrol.*, *120*, 309–325, 1990.

Gutman, G., A simple method for estimating monthly mean albedo from AVHRR data, *J. Appl. Meteorol.*, *27*, 973–988, 1988.

Hobbins, M. T., J. A. Ramírez, and T. C. Brown, The complementary relationship in regional evapotranspiration: The CRAE model and the advection-aridity approach, paper presented at Nineteenth Annual AGU Hydrology Days, AGU, Fort Collins, Colo., 1999.

Hobbins, M. T., J. A. Ramírez, and T. C. Brown, Complementary relationship in the estimation of regional evapotranspiration: An enhanced Advection-Aridity model, *Water Resour. Res.*, this issue.

Kim, C. P., and D. Entekhabi, Examination of two methods for estimating regional evaporation using a coupled mixed layer and land surface model, *Water Resour. Res.*, *33*(9), 2109–2116, 1997.

Kitanidis, P. K., Geostatistics, in *Handbook of Hydrology*, edited by D. R. Maidment, chap. 20, pp. 20.1–20.39, McGraw-Hill, New York, 1992.

Kohler, M. A., and L. H. Parmele, Generalized estimates of free-water evaporation, *Water Resour. Res.*, *3*(4), 997–1005, 1967.

Kovacs, G., Estimation of average areal evapotranspiration—Proposal to modify Morton's model based on the complementary character of actual and potential evapotranspiration, *J. Hydrol.*, *95*, 227–240, 1987.

LeDrew, E. F., A diagnostic examination of a complementary relationship between actual and potential evapotranspiration, *J. Appl. Meteorol.*, *18*, 495–501, 1979.

Lemeur, R., and L. Zhang, Evaluation of three evapotranspiration models in terms of their applicability for an arid region, *J. Hydrol.*, *114*, 395–411, 1990.

Lhomme, J.-P., A theoretical basis for the Priestley-Taylor coefficient, *Boundary Layer Meteorol.*, *82*, 179–191, 1997.

McNaughton, K. G., and T. W. Spriggs, An evaluation of the Priestley and Taylor equation and the complementary relationship using results from a mixed-layer model of the convective boundary layer, in *Estimation of Areal Evapotranspiration*, *IAHS Publ.*, *177*, 89–104, 1989.

Mooty, W. S., and H. H. Jeffcoat, Inventory of inter basin transfer of water in the eastern United States, *U.S. Geol. Surv. Open File Rep.*, *86–148*, 1986.

Morton, F. I., Potential evaporation and river basin evaporation, *J. Hydraul. Div. Am. Soc. Civ. Eng.*, *91*(HY6), 67–97, 1965.

Morton, F. I., Climatological estimates of evapotranspiration, *J. Hydraul. Div. Am. Soc. Civ. Eng.*, *102*(HY3), 275–291, 1976.

Morton, F. I., Operational estimates of areal evapotranspiration and their significance to the science and practice of hydrology, *J. Hydrol.*, *66*, 1–76, 1983.

Morton, F. I., F. Ricard, and S. Fogarasi, Operational estimates of areal evapotranspiration and lake evaporation—Program WREVAP, *Pap. 24*, 75 pp., Natl. Hydrol. Res. Inst., Ottawa, Ont., Canada, 1985.

Nash, J. E., Potential evaporation and "the complementary relationship," *J. Hydrol.*, *111*, 1–7, 1989.

National Oceanic and Atmospheric Administration (NOAA), *Solar and Meteorological Surface Observation Network 1961–1990* [CD-ROM], version 1.0, Natl. Clim. Data Cent., Asheville, N.C., 1993.

Parlange, M. B., and G. G. Katul, Estimation of the diurnal variation of potential evaporation from a wet bare soil surface, *J. Hydrol.*, *132*, 71–89, 1992a.

Parlange, M. B., and G. G. Katul, An advection-aridity evaporation model, *Water Resour. Res.*, *28*(1), 127–132, 1992b.

Penman, H. L., Natural evaporation from open water, bare soil and grass, *Proc. R. Soc. London*, *Ser. A.*, 120–146, 1948.

Petsch, H. E., Jr., Inventory of inter basin transfer of water in the western conterminous United States, *U.S. Geol. Surv. Open File Rep.*, *85–166*, 1985.

Priestley, C. H. B., and R. J. Taylor, On the assessment of surface heat flux and evaporation using large-scale parameters, *Mon. Weather Rev.*, *100*, 81–92, 1972.

Ramírez, J. A., and L. Claessens, Large scale water budgets for the United States, *Final Prog. Rep. Coop. Agreement 28-C2-618*, 153 pp., Hydrol. Sci. and Eng. Dept., Colo. State Univ., Fort Collins, 1994.

Sharma, T. C., An evaluation of evapotranspiration in tropical central Africa, *Hydrol. Sci. J.*, *33*(2), 31–40, 1988.

Slack, J. R., and J. M. Landwehr, Hydro-climatic data network (HCDN): A U.S. Geological Survey streamflow data set for the United States for the study of climate variations, 1874–1988, *U.S. Geol. Surv. Open File Rep.*, *92–129*, 1992.

Tabios, G. Q., and J. D. Salas, A comparative analysis of techniques for spatial interpolation of precipitation, *Water Resour. Bull.*, *21*(3), 365–380, 1985.

U.S. Geological Survey, Class A pan evaporation for period 1931–1960, in *The National Atlas of the United States of America*, 417 pp., Washington, D.C., 1970.

Wallis, J. R., D. P. Lettenmaier, and E. F. Wood, A daily hydroclimatological data set for the continental United States, *Water Resour. Res.*, *27*(7), 1657–1663, 1991.

T. C. Brown, Rocky Mountain Research Station, U.S. Forest Service, Fort Collins, CO 80526-2098. (tcbrown@fs.fed.us)

L. H. J. M. Claessens, The Ecosystems Center, Marine Biological Laboratory, Woods Hole, MA 02543. (lucclaes@mbl.edu)

M. T. Hobbins and J. A. Ramírez, Department of Civil Engineering, Colorado State University, Fort Collins, CO 80523-1372. (mhobbins@lamar.colostate.edu; ramirez@engr.colostate.edu)

(Received December 20, 1999; revised November 2, 2000; accepted November 2, 2000.)